© 2022. Published by The Company of Biologists Ltd | Development (2022) 149, dev200610. doi:10.1242/dev.200610

RESEARCH ARTICLE

Mural Wnt/β-catenin signaling regulates Lama2 expression to promote neurovascular unit maturation

Saptarshi Biswas[1], Sanjid Shahriar[1,2], Nicholas P. Giangreco[3,4], Panos Arvanitis[5], Markus Winkler[6], Nicholas P. Tatonetti[3,4], William J. Brunken[7], Tyler Cutforth[1] and Dritan Agalliu[1,2,*]

ABSTRACT

Neurovascular unit and barrier maturation rely on vascular basement membrane (vBM) composition. Laminins, a major vBM component, are crucial for these processes, yet the signaling pathway(s) that regulate their expression remain unknown. Here, we show that mural cells have active Wnt/β-catenin signaling during central nervous system development in mice. Bulk RNA sequencing and validation using postnatal day 10 and 14 wild-type versus adenomatosis polyposis coli downregulated 1 (*Apcdd1*$^{-/-}$) mouse retinas revealed that Lama2 mRNA and protein levels are increased in mutant vasculature with higher Wnt/β-catenin signaling. Mural cells are the main source of Lama2, and Wnt/β-catenin activation induces Lama2 expression in mural cells *in vitro*. Markers of mature astrocytes, including aquaporin 4 (a water channel in astrocyte endfeet) and integrin-α6 (a laminin receptor), are upregulated in *Apcdd1*$^{-/-}$ retinas with higher Lama2 vBM deposition. Thus, the Wnt/β-catenin pathway regulates Lama2 expression in mural cells to promote neurovascular unit and barrier maturation.

KEY WORDS: Blood–retinal barrier, Canonical Wnt signaling, Laminin, Mural cell, Retina, Vascular basement membrane

INTRODUCTION

In the developing central nervous system (CNS), reciprocal interactions among endothelial cells (ECs), mural cells [pericytes (PCs) and vascular smooth muscle cells (vSMCs)] and glia (astrocytes in the brain; astrocytes and Müller cells in the retina) are crucial to establish the neurovascular unit (NVU) (Biswas et al., 2020; Díaz-Coranguez et al., 2017; Iadecola, 2017). The NVU is essential for neurovascular coupling and the establishment of the blood-brain barrier (BBB) and the blood-retinal barrier (BRB) in the brain and retina, respectively. The BBB/BRB, formed by ECs, ensure a protective milieu for neuronal function (Iadecola, 2017; Liebner et al., 2018). Given that NVU integrity and BBB/BRB properties are perturbed in many cerebrovascular and ocular diseases (Biswas et al., 2020), it is crucial to elucidate how they are established during development.

Interactions among ECs, mural cells and astrocytes via the vascular basement membrane (vBM) are vital for BBB/BRB integrity (Fig. 1A) (Baeten and Akassoglou, 2011; Biswas et al., 2020). Laminins, heterotrimeric glycoproteins made of α-, β- and γ-chains (Durbeej, 2010; Patarroyo et al., 2002), are extracellular matrix (ECM) components with a crucial role in NVU assembly and BBB/BRB properties. Global deletion of the laminin-α2 chain (*Lama2*) (Menezes et al., 2014) or astrocyte-specific deletion of the laminin-γ1 (Lamc1) chain (Chen et al., 2013) cause BBB leakage, hemorrhagic stroke and loss of astrocyte endfeet polarization around blood vessels, and are associated with tight junction disorganization (Yao et al., 2014). Consistent with these phenotypes, neuronal- or glial-specific deletion of dystroglycan, a receptor for laminins, also increases BBB permeability (Menezes et al., 2014). The expression of several integrin receptors or dystroglycan (Paulus et al., 1993), required for attachment of astrocyte endfeet to the vBM, is also regulated by laminins. Loss of either Lama2 (Menezes et al., 2014) or laminin-β2 chain (Gnanaguru et al., 2013) reduces the expression of integrin-β1 in astrocyte endfeet in the brain and delays astrocyte migration in the retina, causing vascular defects and BBB/BRB leakage. Although all NVU cells produce laminins, the precise cellular sources of laminin chains remain controversial. Astrocytes were traditionally thought to be the main source of Lama2 in the cerebral vBM (Sixt et al., 2001); however, recent studies revealed that mural cells are the major source of Lama2 in the brain vBM (Armulik et al., 2010; He et al., 2018; Menezes et al., 2014; Vanlandewijck et al., 2018). Although *Lama2*$^{-/-}$ mice have a disrupted BBB (Menezes et al., 2014), phenocopying mice with loss of endothelial Wnt/β-catenin function, the upstream signaling pathways regulating Lama2 expression and deposition in the vBM are unknown.

Wnt/β-catenin signaling is essential for CNS angiogenesis and BBB/BRB maturation. Loss of Wnt-7a/b ligands or downstream components in ECs perturbs both brain angiogenesis and BBB integrity (Daneman et al., 2009; Liebner et al., 2008; Stenman et al., 2008; Zhou and Nathans, 2014; Zhou et al., 2014). The Wnt/β-catenin pathway also regulates retinal angiogenesis and BRB development through the Norrin-Fzd4-Lrp5/6 signaling module (Wang et al., 2012; Ye et al., 2009; Zhou et al., 2014). Genetic inactivation of *Ndp* (encoding Norrin), *Fzd4*, *Lrp5/6* or Tspan12 receptors in ECs causes delayed retinal angiogenesis, cerebellar hypovascularization and compromised BBB/BRB function (Chen et al., 2012; Junge et al., 2009; Luhmann et al., 2005; Xia et al., 2010; Xu et al., 2004; Ye et al., 2009; Zuercher et al., 2012). Endothelial Wnt/β-catenin signaling promotes BBB/BRB maturation by inducing the expression of tight junction proteins and some transporters (e.g. Slc2a1) and suppressing transcytosis proteins (Biswas et al., 2020). Recent studies also implicated

[1]Department of Neurology, Columbia University Irving Medical Center, New York, NY 10032, USA. [2]Department of Pathology & Cell Biology, Columbia University Irving Medical Center, New York, NY 10032, USA. [3]Department of Systems Biology, Columbia University Irving Medical Center, New York, NY 10032, USA. [4]Department of Biomedical Informatics, Columbia University Irving Medical Center, New York, NY 10032, USA. [5]Department of Biomedical Engineering, Columbia University Irving Medical Center, New York, NY 10032, USA. [6]Faculty of Medicine, Institute of Anatomy, Ludwig-Maximilians Universität, Munich 80336, Germany. [7]Department of Ophthalmology & Visual Sciences, SUNY Upstate Medical University, Syracuse, NY 13210, USA.

*Author for correspondence (da191@cumc.columbia.edu)

D.A., 0000-0002-5375-4143

Handling Editor: James Briscoe
Received 3 February 2022; Accepted 4 August 2022

Development (2022) 149, dev200610. doi:10.1242/dev.200610

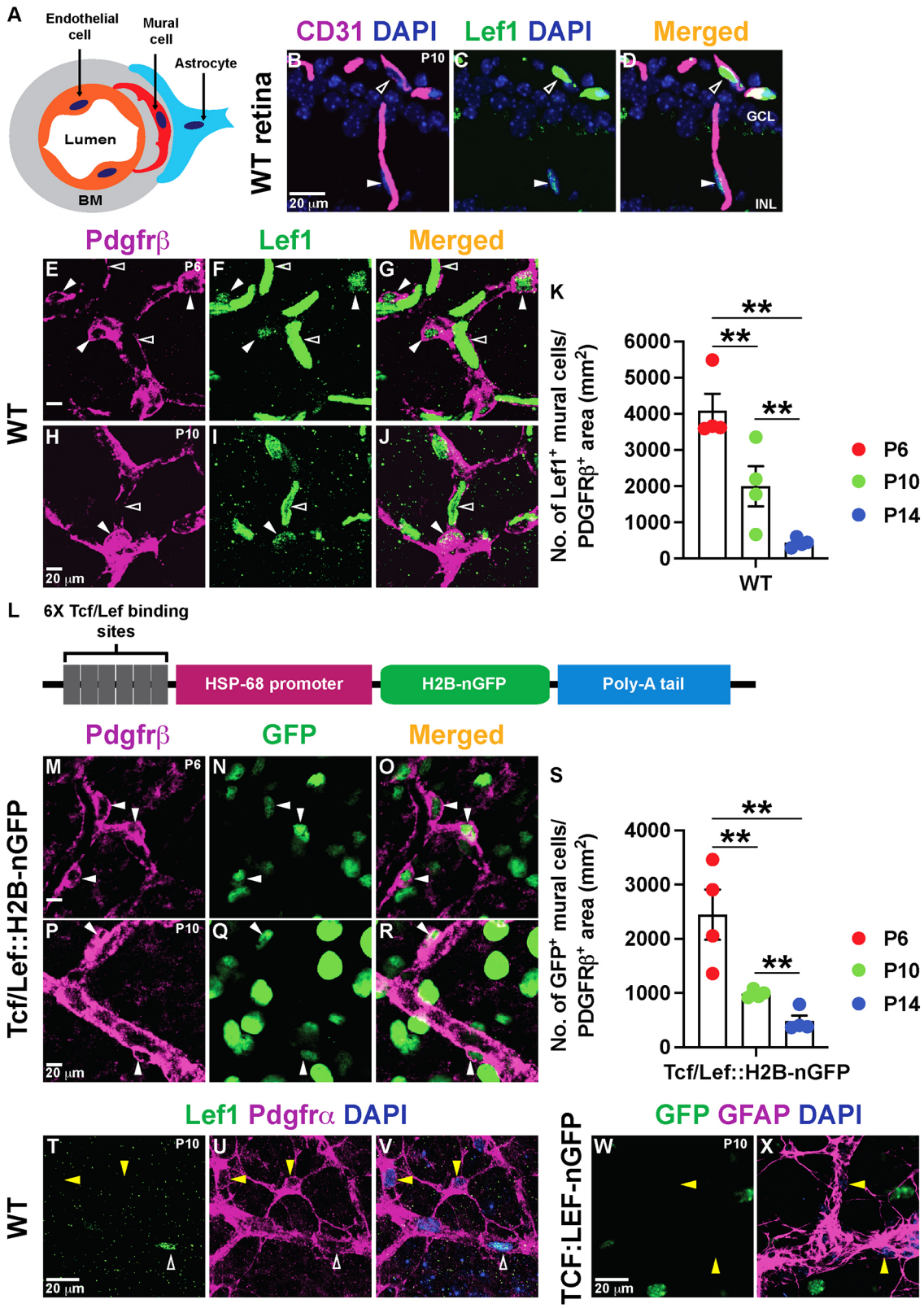

Fig. 1. See next page for legend.

endothelial Wnt/β-catenin signaling in the regulation of collagen IV deposition in the vBM as a result of the activity of Fgfbp1 (Cottarelli et al., 2020). Although the role of endothelial Wnt/β-catenin in CNS angiogenesis and BBB/BRB maturation is well characterized, it is unknown whether this pathway is active in CNS mural cells and how its activity in mural cells affects vBM composition, interactions with ECs and astrocytes, and BBB/BRB development.

In this study, we found that mural cells have active Wnt/β-catenin signaling during CNS development, albeit at levels lower than in ECs. Previously, we have shown that mRNA of the Wnt inhibitor

Development (2022) 149, dev200610. doi:10.1242/dev.200610

Fig. 1. Retinal vascular mural cells have active Norrin/β-catenin signaling. (A) Schematic of the cell types in the NVU. The vBM is depicted in gray. (B-D) P10 WT retinal sections stained for Lef1 (green) and CD31 (magenta). Unfilled arrowheads indicate Lef1$^+$ ECs and filled arrowheads indicate Lef1$^+$ cells next to the ECs in the ganglion cell layer (GCL) and inner nuclear layer (INL). (E-J) Lef1$^+$ ECs (unfilled arrowheads) and Lef1$^+$ mural cells (filled arrowheads) in WT retinal flat-mounts stained for Lef1 (green) and Pdgfrβ (magenta). (K) Lef1$^+$ mural cell numbers in the retina at three developmental time-points (*n*=4/mice per time point). (L) Schematic of the *Tcf/Lef*::H2B-nGFP transgene. (M-R) *Tcf/Lef*::H2B-nGFP retinal flat-mounts labeled for GFP (green) and Pdgfrβ (magenta). Filled arrowheads indicate GFP$^+$ mural cells. (S) GFP$^+$ mural cell numbers in the retina at the indicated developmental time-points (*n*=4/mice per time point). (T-V) P10 WT retinal flat-mounts stained for Lef1, Pdgfrα and DAPI. Yellow arrowheads indicate Lef1$^-$ astrocytes. Unfilled arrowheads indicate Lef1$^+$ ECs. (W,X) P10 *Tcf/Lef*::H2B-nGFP retinal flat-mounts stained for GFP, GFAP and DAPI. Yellow arrowheads indicate GFP$^-$ astrocytes. Data are mean±s.e.m., analyzed with one-way ANOVA with Bonferroni corrections: ***P*<0.02.

adenomatosis polyposis coli downregulated 1 (*Apcdd1*) is expressed by ECs and is essential for coordinating vascular pruning and barrier maturation in the developing retina and cerebellum by modulating Wnt/Norrin signaling (Mazzoni et al., 2017). *Apcdd1*$^{-/-}$ mice exhibit a transient increase in vessel density as a result of delayed vessel pruning, but a precocious maturation in the BBB/BRB (Mazzoni et al., 2017). In this study, we found that *Apcdd1* mRNA is also expressed by mural cells, in addition to ECs. Bulk RNA sequencing (RNA-seq) comparison and validation in wild-type (WT) versus *Apcdd1*$^{-/-}$ retinas, which have higher Wnt/β-catenin signaling in the neurovasculature (Mazzoni et al., 2017), has shown that *Lama2* mRNA and protein are upregulated in the vBM of *Apcdd1*$^{-/-}$ retina and cerebellum. Consistent with mural cells being the main source of Lama2 *in vivo*, we demonstrate that Wnt/β-catenin activation induces *Lama2* expression in retinal mural cells *in vivo* and brain-derived mural cells *in vitro*. Finally, physiological effectors of astrocytic homeostasis, including integrin-α6 (Itga6; a laminin receptor) and aquaporin 4 (Aqp4; localized in polarized astrocyte endfeet), are upregulated in *Apcdd1*$^{-/-}$ retinal blood vessels. Our findings reveal that Wnt/β-catenin activation in mural cells regulates Lama2 expression to promote NVU, astrocyte and neurovascular barrier maturation.

RESULTS

Retinal and cerebellar mural cells have active Wnt/β-catenin signaling

Although Wnt/β-catenin activity is well characterized in CNS ECs, its role in other NVU cells remains unknown. To determine whether Wnt/β-catenin signaling is active in other NVU cells, we examined the expression of Lef1, a downstream target and readout of pathway activation (Fancy et al., 2014). Lef1 was expressed at high levels in WT retinal ECs (CD31; Fig. 1B-J, unfilled arrowheads) and at lower levels in Pdgfrβ$^+$ mural cells (Fig. 1B-J, filled arrowheads) in the developing retina. The number of Lef1$^+$ cells within the Pdgfrβ$^+$ area decreased significantly from postnatal day (P) 6 to P14 (Fig. 1K) as the BRB matured. We confirmed these findings in *Tcf/Lef*::H2B-nGFP transgenic mice, in which nuclear GFP expression is under the control of Wnt/β-catenin activity (Fig. 1L) (Ferrer-Vaquer et al., 2010; Lengfeld et al., 2017). Nuclear GFP was present in Pdgfrβ$^+$ retinal mural cells (Fig. 1M-R, filled arrowheads), and their number decreased from P6 to P14 (Fig. 1S). In contrast, Lef1 (WT) and GFP (*Tcf/Lef*::H2B-nGFP) were not expressed by astrocytes (Pdgfrα$^+$ or GFAP$^+$) in the retina (Fig. 1T-X, yellow arrowheads), suggesting the absence of Wnt/β-catenin signaling. Nuclear GFP was also present in neurons of the *Tcf/Lef*::H2B-nGFP retinas (Fig. 1M-R), consistent with published single-cell RNA-seq data from P14 retina (https://singlecell.broadinstitute.org/single_cell/study/SCP301/c57b6-wild-type-p14-retina-by-drop-seq#study-summary) (Macosko et al., 2015). Finally, we analyzed expression of Apcdd1, a target and negative regulator of Wnt/β-catenin signaling (Mazzoni et al., 2017; Shimomura et al., 2010) in ECs and mural cells in the retina. Fluorescence RNA *in situ* hybridization (FISH) with antisense mRNA probes against *Apcdd1* along with immunostaining for caveolin 1 (ECs), Pdgfrβ (mural cells) and GFAP (astrocytes) at both P6 (Fig. S1F-K) and P10 retinas demonstrated that *Apcdd1* colocalized with ∼97% of ECs (Fig. 2A,D, filled arrowhead) and ∼73% of mural cells (Fig. 2B,D, filled arrowhead) at P10, whereas astrocytes expressed almost no *Apcdd1* (Fig. 2C,D, asterisks). Similarly, analysis of the P14 retinal single-cell RNA-seq database (Macosko et al., 2015) confirmed that three Wnt/β-catenin targets (*Lef1*, *Apcdd1* and *Axin2*) are expressed at high levels in ECs and lower levels in mural cells, but are absent in astrocytes (Fig. S1A). Among distinct vessel subtypes in the retina, mural cells around arteries and veins showed higher levels of Wnt/β-catenin activation compared with those around capillaries (Fig. S1B-E).

Norrin is crucial for angiogenesis and barrier maturation in both the developing retina and cerebellum (Wang et al., 2018, 2012; Zhou et al., 2014). Similar to the retina, developing P3 cerebellar Foxc1$^+$ mural cells (Siegenthaler et al., 2013) had low Lef1 levels (Foxc1$^+$ Lef1^{low}; Fig. S2A-B′, filled arrowhead), in contrast to Foxc1$^-$ Lef1^{high} ECs (Fig. S2A-B′, unfilled arrowhead). P10 cerebellar Pdgfrβ$^+$ mural cells also had low Lef1 expression (Fig. S2C-D′, filled arrowhead). We found similar results in P10 and P14 *Tcf/Lef*::H2B-nGFP cerebella, in which Pdgfrβ$^+$ mural cells expressed low nGFP (Fig. S2E-H′, filled arrowheads). We also examined Wnt/β-catenin signaling activation in mural cells in the cerebral cortex, in which Wnt 7a/7b are the main Wnt ligands (Daneman et al., 2009; Liebner et al., 2008; Zhou et al., 2014), and found Lef1$^+$ mural cells in the cortex at P10 (Fig. S2I-J′, filled arrowheads). In summary, mural cells have active Wnt/β-catenin signaling in the CNS, albeit at lower levels than in ECs. Moreover, Wnt/β-catenin activity decreases gradually in mural cells as the BBB/BRB matures.

Lama2, expressed by mural cells, is upregulated in the *Apcdd1*$^{-/-}$ retinal vBM

We have previously shown that global deletion of Apcdd1 (*Apcdd1*$^{-/-}$) leads to precocious BRB and BBB (cerebellum) maturation between P10 and P14 as a result of upregulation of Wnt/β-catenin activity (Mazzoni et al., 2017). Given that *Apcdd1* mRNA is expressed by both ECs and PCs, to understand how Apcdd1 regulates BRB/BBB maturation, we performed a bulk mRNA-seq between WT and *Apcdd1*$^{-/-}$ retinas at P10 and P14, to identify differentially expressed transcripts. Putative retinal EC or mural cell sources for Apcdd1-regulated transcripts were assigned using the P14 retinal single-cell RNA-seq database (Macosko et al., 2015). Finally, differentially expressed gene lists and volcano plots were constructed for each cell type and pathway category (Fig. 2E-J; Tables S1-S5). This analysis revealed that several EC-specific genes were differentially expressed between WT and *Apcdd1*$^{-/-}$ retinas at both P10 and P14 (Fig. 2E,F; Tables S1, S2), consistent with high *Apcdd1* mRNA expression in retinal ECs (Mazzoni et al., 2017). Interestingly, many PC-specific genes were also differentially expressed between WT and *Apcdd1*$^{-/-}$ retinas at both developmental stages (Fig. 2G,H; Tables S1, S3), consistent with *Apcdd1* mRNA expression in a subset of mural cells (Fig. 2A-D;

Development (2022) 149, dev200610. doi:10.1242/dev.200610

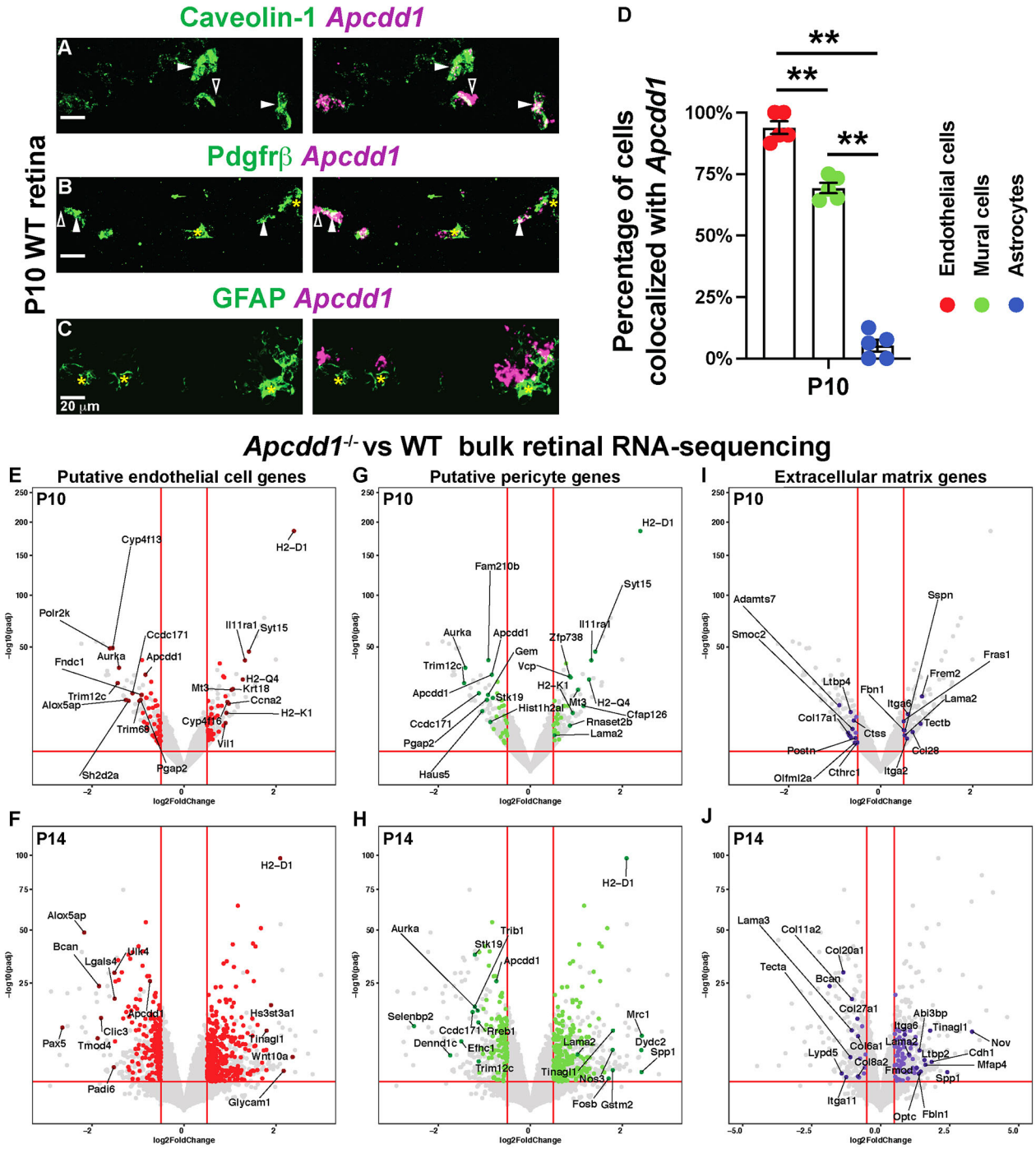

Fig. 2. *Apcdd1* is expressed in both retinal ECs and PCs and *Lama2* expression is increased in *Apcdd1*$^{-/-}$ retinas. (A-C) FISH of P10 WT retinal sections with antisense mRNA probes against *Apcdd1* (magenta) followed by immunostaining for caveolin 1, Pdgfrβ or GFAP (green). Filled arrowheads, asterisks and unfilled arrowheads indicate *Apcdd1* inside the cell, *Apcdd1*$^{-}$ cells and *Apcdd1* outside the cell, respectively. (D) Fraction of *Apcdd1*$^{+}$ ECs, mural cells and astrocytes in the retina (n=4 mice). (E-J) Volcano plots of putative EC (E,F: red dots), PC (G,H: green dots) and ECM (I,J; purple dots) genes differentially expressed between P10 and P14 *Apcdd1*$^{-/-}$ and WT retinas. Genes above the horizontal red lines are those with significantly different expression in *Apcdd1*$^{-/-}$ retinas. Genes to the right of vertical red lines are significantly upregulated, whereas those to the left are significantly downregulated in *Apcdd1*$^{-/-}$ retinas. The most differentially expressed genes are named. Data are mean±s.e.m., analyzed with two-tailed unpaired Student's *t*-test: $^{**}P$<0.02.

Fig. S1F-K) and upregulation of Wnt/β-catenin activity in *Apcdd1*$^{-/-}$ retinal mural cells, indicated by increased Lef1 expression (Fig. S3A-C).

Among the ECM genes, *Lama2* and *Itga6* transcripts were upregulated in both P10 and P14 *Apcdd1*$^{-/-}$ retinas (Fig. 2G-J; Tables S1, S3, S4). In contrast, other ECM genes, such as *Lama1*, *Lama4* and *Lama5* (encoding laminin-α1, -α4 and -α5, respectively) or *Col4a1* and *Col4a2* (encoding collagen IV subunits), were not significantly different between the two genotypes (Tables S1, S4). Given that *Apcdd1* is expressed by both ECs and mural cells, we examined which cell type produces *Lama2* mRNA. FISH with an antisense mRNA probe against *Lama2*, followed by

Development (2022) 149, dev200610. doi:10.1242/dev.200610

immunolabeling with cell markers, showed that the majority of vessel-associated *Lama2* mRNA colocalized with NG2$^+$ mural cells (Fig. 3A, filled arrowheads) in the P10 WT retina, along with partial colocalization with GFAP$^+$ astrocytes (Fig. 3C). In contrast, *Lama2* did not colocalize with caveolin 1$^+$ ECs (Fig. 3B, unfilled arrowheads). These data were confirmed in P14 *Lama2*$^{lacZ/+}$ reporter retinas, in which *lacZ*, which encodes β-galactosidase (β-Gal) protein is inserted into the *Lama2* locus (Kuang et al., 1998), with markers for mural cells (NG2), ECs (lectin) and astrocytes (GFAP). Vascular β-Gal colocalized with NG2$^+$ mural cells (Fig. 3D, filled arrowheads), but not lectin$^+$ ECs (Fig. 3E, unfilled arrowheads). The astrocyte marker GFAP also partially colocalized with vascular β-Gal (Fig. 3F). Extravascular β-Gal expression is likely in retinal neurons or Müller glia (Macosko et al., 2015); however, these cell types do not contribute to the deposition of Lama2 in the vBM of the superficial vascular plexus (Biswas et al., 2020). These results are consistent with P14 retinal single-cell RNA-seq data (Macosko et al., 2015), which showed that mural cells, specifically PCs, are the predominant source of *Lama2* in the P14 retina (Fig. S3D). Similar to the retina, β-Gal was also localized with NG2$^+$ mural cells (Fig. S4C,D, filled arrowheads), but not with lectin$^+$ ECs (Fig. S4A, B, unfilled arrowheads), in cerebellar blood vessels of *Lama2*$^{lacZ/+}$ reporter mice, a finding consistent with brain single-cell RNA-seq studies showing that mural, but not endothelial, cells express *Lama2* (Armulik et al., 2010; He et al., 2018; Menezes et al., 2014; Vanlandewijck et al., 2018).

To validate our bulk RNA-seq data with regard to increased *Lama2* mRNA expression in *Apcdd1*$^{-/-}$ mural cells, we performed FISH with antisense probe against *Lama2*, followed by immunolabeling with cell markers in P14 WT and *Apcdd1*$^{-/-}$ retinas. The mean fluorescence intensity (M.F.I.) of *Lama2* puncta was higher in *Apcdd1*$^{-/-}$ compared with WT retinal mural cells (Fig. 3G,H), supporting the bulk RNA-seq data (Fig. 2G,H; Tables S3, S4). In contrast, the fluorescence intensity of *Lama2* puncta did not change in *Apcdd1*$^{-/-}$ compared with WT retinal ECs and astrocytes (Fig. 3I-L). Next, we examined Lama2 protein deposition to the vBM of WT and *Apcdd1*$^{-/-}$ retinas. We used CD31 M.F.I. to normalize the Lama2 fluorescence signal in the vBM because CD31 M.F.I. did not change between the two genotypes (Fig. 3M-P). Quantification of Lama2 relative to CD31 M.F.I. in retinal vessels revealed that Lama2 deposition was upregulated by ∼25% in P10 arterial, but not venous, vBM (Fig. 3O, P), and by ∼30% in P14 arterial and venous vBMs (Fig. 3M-P) of *Apcdd1*$^{-/-}$ compared with WT retinas. The effects were more pronounced in arteries because Lama2 protein deposition is normally lower in arterial compared with venous vBM in P14 retina (Fig. S3E,F). In contrast to arteries and veins, Lama2 protein deposition did not change in the capillary vBM between P14 *Apcdd1*$^{-/-}$ and WT retinas (Fig. S3G-K), consistent with the lower level of Wnt/β-catenin activity in mural cells surrounding capillaries compared with arteries and veins (Fig. S1B-E). Western blot analyses of Lama1 and Lama2 also showed higher Lama2 levels in P14 *Apcdd1*$^{-/-}$ compared with WT retina, whereas Lama1 levels were similar (Fig. S3L-N). Quantification of Lama2 intensity relative to CD31 in cerebellar blood vessels also showed a 2-fold increase in vBM deposition in P14 *Apcdd1*$^{-/-}$ compared with WT mice (Fig. S4E-I). In summary, although both ECs and mural cells have active Wnt/β-catenin signaling, only mural cells express *Lama2*. Retinal astrocytes also express *Lama2*; however, they do not have active Wnt/β-catenin signaling. Thus, loss of Apcdd1 leads to increased *Lama2* mRNA and protein expression by mural cells and deposition to the retinal and cerebellar vBMs.

To confirm the relationship between Lama2 deposition to the vBM and neurovascular barrier maturation, we analyzed paracellular BRB permeability in *Lama2*$^{-/-}$ mice (Kuang et al., 1998). We quantified the accumulation of biocytin-tetramethylrhodamine (biocytin-TMR), an 870 Da tracer that crosses the leaky or immature BBB/BRB (Lengfeld et al., 2017; Mazzoni et al., 2017), into the *Lama2*$^{-/-}$ and WT CNS parenchyma, 30 min after intravenous injection. There was a 5.5-fold increase in biocytin-TMR M.F.I. in both central and peripheral *Lama2*$^{-/-}$ compared with WT retinas (Fig. 4A-F), indicative of a leaky BRB. In addition, expression of the tight junction protein occludin was significantly reduced in *Lama2*$^{-/-}$ retinas (Fig. 4G-K). This is consistent with a previous study showing increased BBB leakage and loss of tight junction proteins in *Lama2*$^{-/-}$ brain (Menezes et al., 2014). The leaky *Lama2* $^{-/-}$ BRB phenotype was opposite to that of the *Apcdd1*$^{-/-}$ retina, in which paracellular BRB is precociously mature (Fig. 4L), occludin levels are increased in ECs (Mazzoni et al., 2017) and Lama2 deposition is upregulated in the vBM (Fig. 3; Fig. S3).

Wnt/β-catenin signaling directly regulates Lama2 expression by mural cells

The above data suggest that precocious BBB/BRB maturation in *Apcdd1*$^{-/-}$ cerebella and retinas (Mazzoni et al., 2017), is caused, in part, by higher Lama2 levels in the vBM resulting from increased Wnt/β-catenin activity in mural cells. To test this hypothesis, we cultured primary purified brain PCs, astrocytes and ECs plated onto poly-D-lysine (PDL)-coated dishes, in the presence of either DMSO (control) or the Wnt agonist CHIR99021 (1.0 µM) (Tran and Zheng, 2017) for 48 h and analyzed the expression of Lef1 and Lama2. CHIR99021 increased expression and nuclear localization of Lef1 by ∼3-fold (Fig. 5A,B) and increased Lama2 expression by ∼2-fold (Fig. 5C,D) in primary brain PCs (Pdgfrβ$^+$ or NG2$^+$ cells) *in vitro* within 48 h. In contrast, there was neither Lef1 expression (Fig. 5E,F) nor a change in Lama2 secretion (Fig. 5G,H) in astrocytes (Pdgfrα$^+$ or GFAP$^+$) in response to either DMSO or CHIR treatment. Although ECs (lectin$^+$) showed upregulated Lef1 expression with CHIR99021 treatment (Fig. 5I,J), they did not express any Lama2 (Fig. 5K,L). We repeated this experiment with recombinant Wnt3a (Cottarelli et al., 2020; Mazzoni et al., 2017), and found similar results to those seen with CHIR99021 treatment (Fig. 5M-R). These data suggest that Wnt/β-catenin signaling induces Lama2 expression and secretion by mural cells, but not by astrocytes or ECs.

We next sought to identify which α2 chain-containing laminin trimer is affected in the *Apcdd1*$^{-/-}$ retina. Three laminin trimers contain the α2 chain: laminin-211 (α2, β1 and γ1), −221 (α2, β2 and γ1) and −213 (α2, β1 and γ3) (Patarroyo et al., 2002) (Fig. S5A,J). Previous studies have reported that loss of the Lamc1 chain in PCs leads to BBB leakage (Gautam et al., 2016), whereas loss of the laminin-γ3 chain does not affect BRB integrity (Gnanaguru et al., 2013). Moreover, the laminin-γ3 chain is almost absent in the arterial vBM of P12 retinas (Biswas et al., 2018); thus, laminin-213 is unlikely to contribute to the increase in α2 chain-containing laminin trimer deposition in the *Apcdd1*$^{-/-}$ retinal vBM.

To distinguish between the remaining laminin trimers (laminin-211 and 221), we examined vBM deposition of laminin-β1 and -β2 chains in both WT and *Apcdd1*$^{-/-}$ retinas. The deposition of laminin-β1 chains followed a similar pattern to that of Lama2α; that is, it was upregulated primarily in the arterial (∼30%) and to a smaller extent in the venous (∼10%) vBM in *Apcdd1*$^{-/-}$ compared with WT retinas (Fig. S5B-I,S,T). In contrast, the vBM deposition

Development (2022) 149, dev200610. doi:10.1242/dev.200610

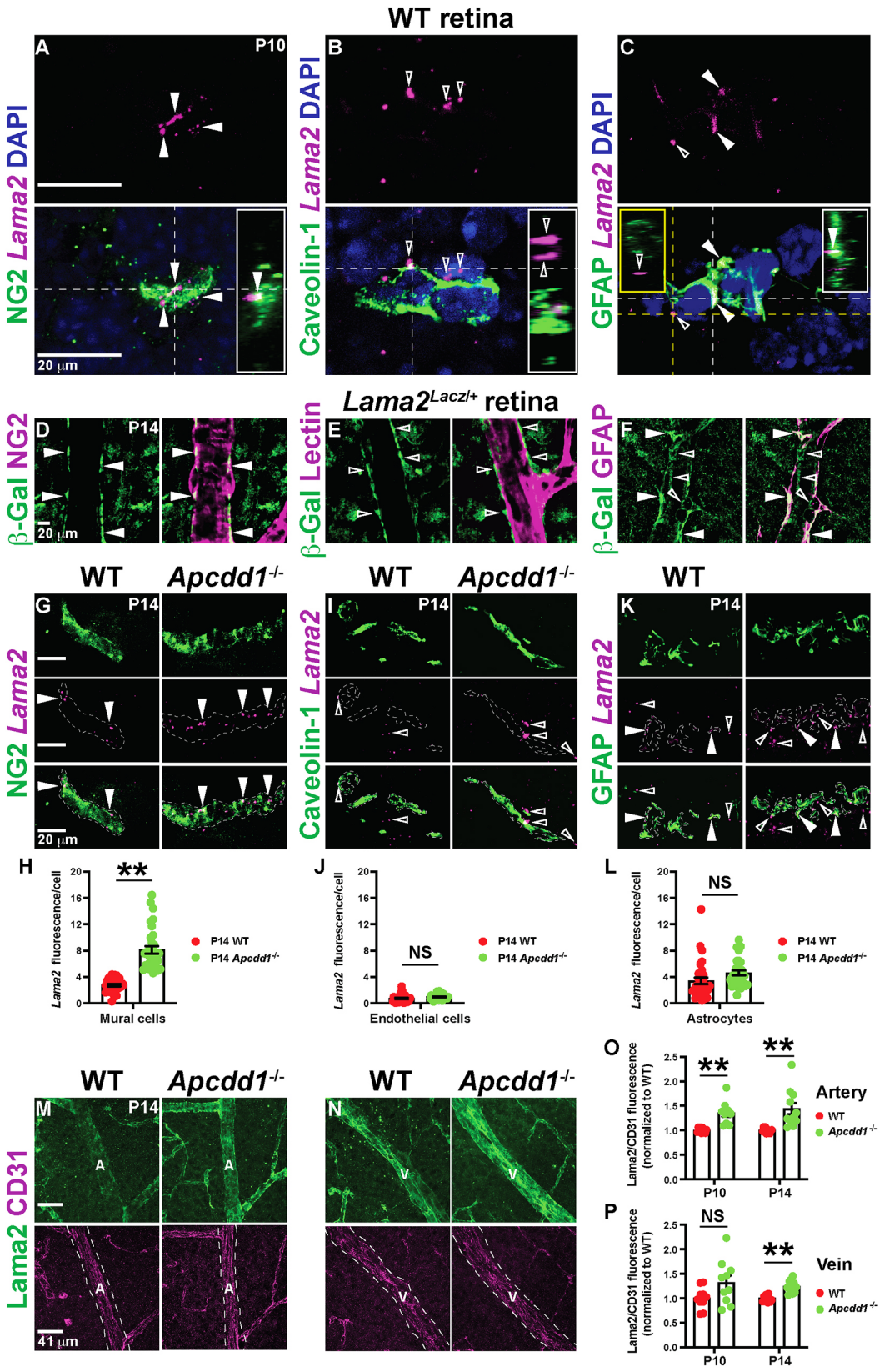

Fig. 3. See next page for legend.

of the laminin-β2 chain in the retina did not differ between the two genotypes (Fig. S5K-R,U,V). The P14 retinal single-cell RNA-seq database (Macosko et al., 2015) confirmed that mural cells are the main source of *Lamb1* and *Lamc1*, whereas *Lamb2* is predominantly expressed by astrocytes (Fig. S5W). Thus, Apcdd1-mediated modulation of Wnt/β-catenin signaling in mural cells regulates Lama2 deposition to the retinal vBM, with Laminin-211 likely being the most affected laminin trimer.

Development (2022) 149, dev200610. doi:10.1242/dev.200610

Fig. 3. *Lama2* expression in mural cells and Lama2 deposition to the vBM is increased in *Apcdd1*$^{-/-}$ retinas. (A-C) FISH of P10 WT retinal sections with antisense probes against *Lama2* (magenta) followed by immunostaining for NG2, caveolin 1 or GFAP (green) and DAPI (blue). Filled and unfilled arrowheads indicate *Lama2* expression inside and outside cells, respectively. Insets show orthogonal projections of the area intersected by corresponding colored lines. (D-F) P14 *Lama2*$^{lacZ/+}$ retinal flat-mounts stained for β-Gal and either NG2, lectin or GFAP. Filled and unfilled arrowheads indicate β-Gal localization inside and outside the cell, respectively. (G,I,K) FISH of P14 WT and *Apcdd1*$^{-/-}$retinal sections with antisense probes against *Lama2* (magenta) followed by immunostaining for NG2, caveolin 1 or GFAP (green). Filled and unfilled arrowheads indicate *Lama2* localization inside and outside the cell, respectively. (H,J,L) *Lama2* M.F.I. within each cell marker between WT and *Apcdd1*$^{-/-}$ retinas (32 fields from *n*=4 mice/genotype). (M,N) P14 WT and *Apcdd1*$^{-/-}$ retinal flat-mounts stained for Lama2 and CD31. Arteries (A) and veins (V) are outlined by dashed white lines. (O,P) Ratio of Lama2/CD31 M.F.I. in arteries and veins normalized to the WT average values at P10 and P14 (ten arteries or veins from *n*=5 mice/genotype). Data are mean±s.e.m., analyzed with two-tailed unpaired Student's *t*-test: NS, not significant, ***P*<0.02.

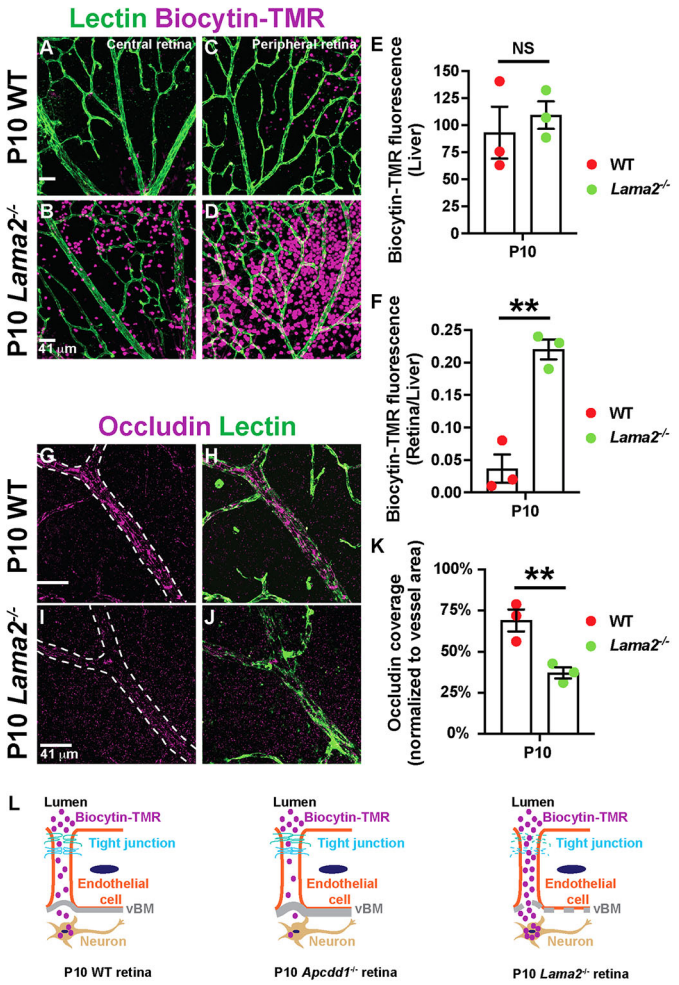

Fig. 4. Paracellular BRB permeability is increased in *Lama2*$^{-/-}$ retinas. (A-D) P10 WT and *Lama2*$^{-/-}$ retinal flat-mounts, injected with biocytin-TMR, stained for lectin. (E,F) Biocytin-TMR M.F.I. in the liver parenchyma (E) and the ratio of biocytin-TMR fluorescence intensities in the retina versus liver parenchyma (F) (*n*=3 mice/genotype). (G-J) P10 WT and *Lama2*$^{-/-}$ retinal flat-mounts stained for occludin and lectin. (K) Occludin coverage of blood vessels (*n*=3 mice/genotype). (L) Schematic of paracellular biocytin-TMR extravasation in WT, *Apcdd1*$^{-/-}$ and *Lama2*$^{-/-}$ retinas. Data are mean±s.e.m., analyzed with two-tailed unpaired Student's *t*-test: NS, not significant, ***P*<0.02.

Astrocytes mature precociously in the *Apcdd1*$^{-/-}$ retina

Next, we asked whether NVU maturation is affected in response to increased Lama2 deposition in *Apcdd1*$^{-/-}$ retinal vBM. We have previously shown that loss of Apcdd1 does not affect mural cell coverage of retinal vessels (Mazzoni et al., 2017). Given that astrocytes adhere to the vBM through their endfeet and changes in the vBM composition affect astrocyte homeostasis (Armulik et al., 2010; Menezes et al., 2014), we asked whether astrocyte maturation and polarization are affected in response to increased Lama2 deposition into the *Apcdd1*$^{-/-}$ retinal vBM. Our bulk RNA-seq data showed that several transcripts expressed by mature astrocytes (e.g. *Mlc1*, *Apoe*, *Gja1* and *Gfap*) (Li et al., 2019; Tao and Zhang, 2014) were upregulated in *Apcdd1*$^{-/-}$ retinas only at P14, with the exception of two transcripts, *Plcd4* and *Aqp4* (Li et al., 2019), which were also upregulated in P10 *Apcdd1*$^{-/-}$ retina (Fig. 6A,B; Table S5). In contrast, the transcript for an immature astrocyte marker, *Sh3pxd2b* (Li et al., 2019), was downregulated in P14 *Apcdd1*$^{-/-}$ retina (Fig. 6B). Thus, transcriptional changes related to astrocyte maturation become significant at a later developmental stage compared with those in either ECs or mural cells in *Apcdd1*$^{-/-}$ retinas.

To validate these bulk RNA-seq findings, we labeled P14 WT and *Apcdd1*$^{-/-}$ retinas for Pdgfrα and GFAP, marking all and mature astrocytes, respectively (Tao and Zhang, 2014). Although Pdgfrα^{+} astrocyte coverage was unchanged, GFAP M.F.I. immunoreactivity was increased by ∼30% in *Apcdd1*$^{-/-}$ compared with WT retinas (Fig. 6C-J). Müller glia, which span the thickness of the retina, also upregulate GFAP expression during gliosis (Iandiev et al., 2006), prompting us to examine whether Müller gliosis contributes to increased GFAP expression in *Apcdd1*$^{-/-}$ retinas. GFAP was detected only in astrocytes over the ganglion cell layer in both P14 WT and *Apcdd1*$^{-/-}$ retinas, with no expression in deeper layers in which Müller cell bodies and processes are located (Fig. 6K,L). Thus, GFAP upregulation in the *Apcdd1*$^{-/-}$ retina occurs exclusively in astrocytes.

GFAP upregulation may indicate reactive astrogliosis, prompting us to examine the expression of established reactive astrogliosis markers (Escartin et al., 2021). However, there was no upregulation in expression of several reactive astrocyte markers (e.g. Nes, Synm, Vim, C3, Aldoc, Blbp, Maob, Lcn2, Serpina3, S100b, Sox9, Stat3, Trkb, Eaat1, Eaat2 or Kir4.1; Table S1) in *Apcdd1*$^{-/-}$ retinal astrocytes. Therefore, retinal astrocytes mature precociously in *Apcdd1*$^{-/-}$ retinas between P10 and P14, in parallel with precocious BRB maturation (Mazzoni et al., 2017).

Next, we examined astrocyte endfeet polarization around retinal blood vessels. Aqp4, a water channel protein expressed by mature astrocytes (Li et al., 2019), exhibits polarized expression in astrocyte endfeet surrounding blood vessels. Total Aqp4 protein levels revealed by western blot were significantly upregulated in *Apcdd1*$^{-/-}$ compared with WT retinas (Fig. S6A,B). Next, we labeled WT and *Apcdd1*$^{-/-}$ retinas with Aqp4 and CD31, and quantified the percentage of vessel length covered by Aqp4^{+} astrocyte endfeet. Aqp4^{+} astrocyte endfeet coverage of retinal vessels increased by ∼45% in P14 *Apcdd1*$^{-/-}$ compared with WT mice (Fig. 6M-V). We confirmed these findings with transmission electron microscopy (TEM), which revealed more extensive astrocyte endfeet coverage, specifically around arteries and veins, in the P14 *Apcdd1*$^{-/-}$ retina compared with WT retina (Fig. 7A-F). Interestingly, there was no obvious difference in vBM thickness between *Apcdd1*$^{-/-}$ and WT retinas, most likely the result of a modest change only in Lama2 deposition (data not shown). Endothelial tight junction ultrastructure was also unaffected in the *Apcdd1*$^{-/-}$ retina (Fig. 7G,H).

Development (2022) 149, dev200610. doi:10.1242/dev.200610

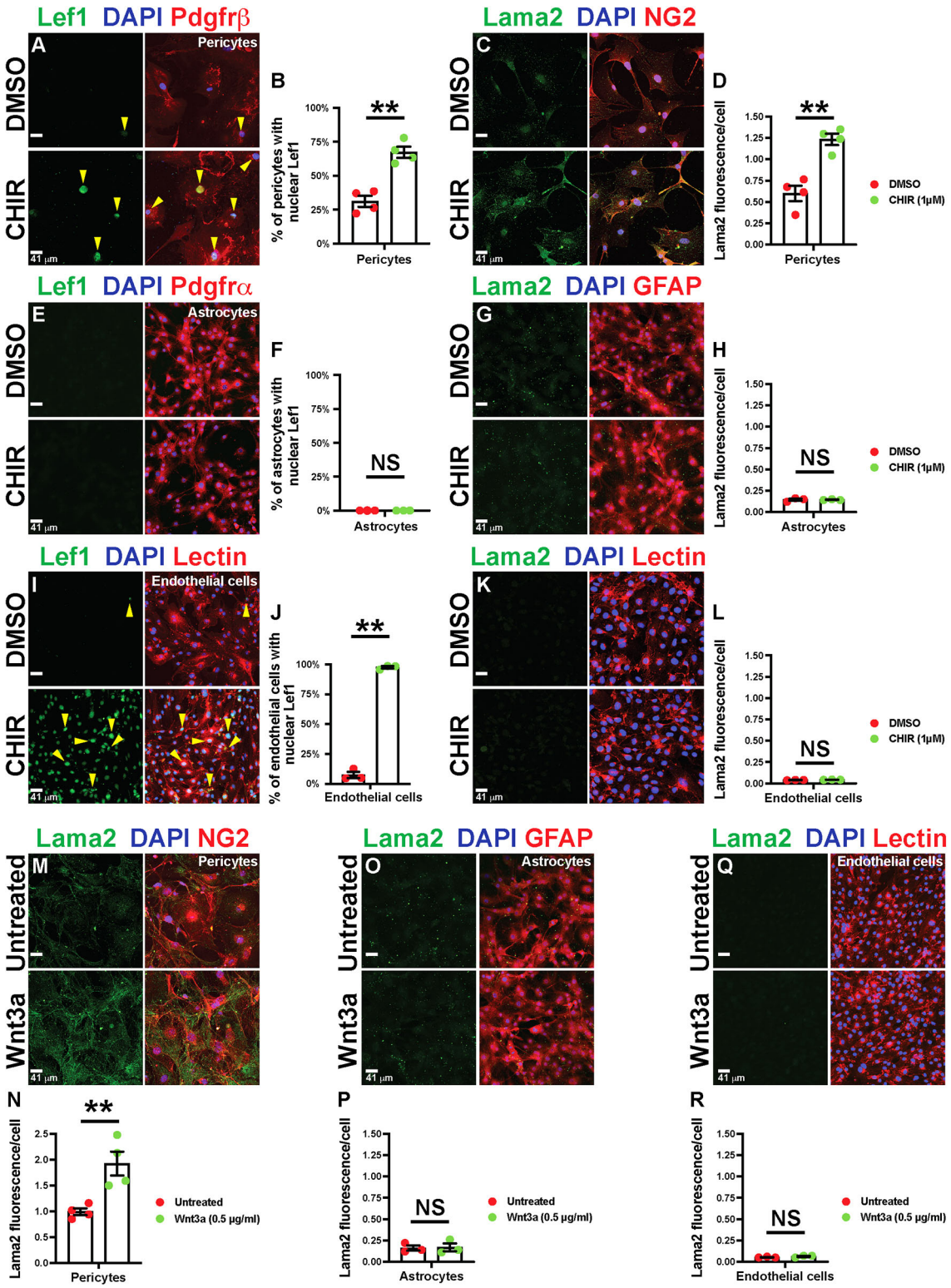

Fig. 5. Wnt/β-catenin activation upregulates Lama2 expression in PCs, but not in astrocytes and ECs. (A-L) Primary mouse brain PCs, astrocytes and ECs treated with either DMSO or CHIR99021 (CHIR), followed by staining for Lef1, DAPI and either Pdgfrβ, Pdgfrα or lectin (A,E,I), or Lama2, DAPI and either NG2, GFAP or lectin (C,G,K). Yellow arrowheads indicate Lef1^{+} nuclei. B,F,J show percentage of cells with nuclear Lef1 expression. H,J,L show quantification of Lama2 expression by corresponding cell types. (M-R) Untreated or recombinant Wnt3a-treated primary mouse brain PCs, astrocytes and ECs stained for Lama2, DAPI and then NG2 (M), GFAP (O) or lectin (Q). N,P,R show the quantification of Lama2 expression by various cell types. *n*=3 or 4 independent experiments; Data are mean±s.e.m., analyzed with two-tailed unpaired Student's *t*-test: NS, not significant, ***P*<0.02.

These data suggest a causal relationship between increased Lama2 expression and precocious astrocyte maturation and endfeet polarization in *Apcdd1*$^{-/-}$ retinas. To confirm this relationship, we examined astrocyte maturation and polarization in *Lama2*$^{-/-}$ retinas. Polarized expression of Aqp4 in astrocyte endfeet around superficial plexus blood vessels was drastically reduced in the

Development (2022) 149, dev200610. doi:10.1242/dev.200610

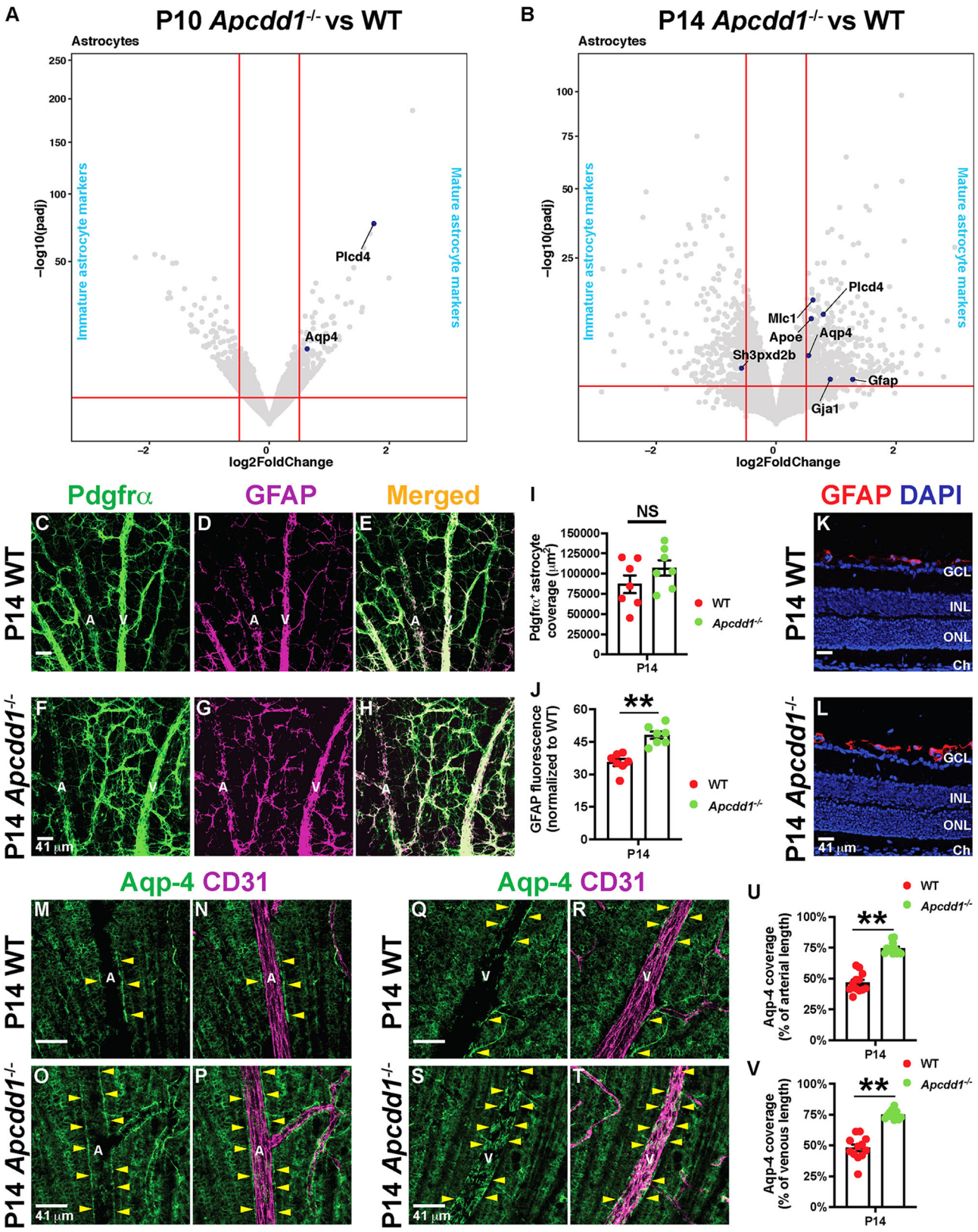

Fig. 6. *Apcdd1*$^{-/-}$ retinas show precocious astrocyte maturation and endfeet polarization. (A,B) Volcano plots of statistically significant differentially expressed astrocyte maturation genes (dark blue dots) between *Apcdd1*$^{-/-}$ and WT retinas at P10 and P14. Conventions as outlined in Fig. 2E-J. (C-H) P14 WT and *Apcdd1*$^{-/-}$ retinal flat-mounts stained for Pdgfrα (all astrocytes) and GFAP (mature astrocytes). (I,J) Pdgfrα^{+} astrocyte coverage (I) and GFAP M.F.I. (J) (n=7 mice/genotype). (K,L) P14 WT (K) and *Apcdd1*$^{-/-}$ (L) retinal sections stained for GFAP and DAPI. (M-T) P14 WT and *Apcdd1*$^{-/-}$ retinal flat-mounts stained for Aqp4 and CD31 in arteries (M-P) and veins (Q-T). A, artery; V, vein. Yellow arrowheads indicate Aqp4^{+} astrocyte endfeet around blood vessels. (U,V) Percentage of vascular length surrounded by Aqp4^{+} astrocyte endfeet (12 arteries or veins from n=6 mice/group). Data are mean±s.e.m., analyzed with two-tailed unpaired Student's t-test: NS, not significant, **P<0.02.

Development (2022) 149, dev200610. doi:10.1242/dev.200610

Lama2$^{-/-}$ retina (Fig. S6C-F), consistent with previous findings in the brain (Menezes et al., 2014). Similar to the retina, Aqp4 immunoreactivity was also increased in astrocyte endfeet around *Apcdd1*$^{-/-}$ cerebellar vessels (Fig. S7A-F). Given the crucial role of polarized Aqp4 expression in maintaining BRB integrity (Nicchia et al., 2004), these data explain, in part, the precocious BRB maturation in the *Apcdd1*$^{-/-}$ retina, and the opposite phenotype in the *Lama2*$^{-/-}$ retina. Thus, the amount of Lama2 deposition in the vBM affects the timing of astrocyte maturation and polarization in the developing CNS.

Astrocytic expression of Itga6 is increased in *Apcdd1*$^{-/-}$ retina to compensate for Lama2 levels and promotes their maturation

Next, we asked how astrocyte maturation is accelerated in the *Apcdd1*$^{-/-}$ retina. We examined expression of Lef1 and found that it was absent in P10 *Apcdd1*$^{-/-}$ retinal astrocytes (Fig. 8A, yellow arrowhead), indicative of no aberrant Wnt/β-catenin signaling activation by *Apcdd1*$^{-/-}$ retinal astrocytes. We hypothesized that astrocyte maturation in the *Apcdd1*$^{-/-}$ retina is accelerated as a result of increased adhesion to the vBM in response to higher Lama2 levels. Previous studies have shown that several ECM receptors, including integrin-α2, -α6, -β1 and -β4 chains expressed by astrocytes (Gnanaguru et al., 2013; Nirwane and Yao, 2018), are affected by changes in vBM protein composition. Integrin-β1 expression at the gliovascular interphase is significantly decreased in the *Lama2*$^{-/-}$ brain, and blocking integrin-β1-mediated adhesion in astrocytes significantly decreases Aqp4 clustering at the cell-ECM interphase (Menezes et al., 2014); however, the α-partner of integrin-β1 responsible for this process was not identified. Given that *Apcdd1*$^{-/-}$ retina exhibits an opposite phenotype to that of *Lama2*$^{-/-}$ retina, we hypothesized that astrocytic integrin expression increases in response to higher levels of Lama2 in the vBM. Consistent with this hypothesis, our bulk RNA-seq data revealed that *Itga6* levels were significantly increased in the *Apcdd1*$^{-/-}$ retina at both P10 and P14 (Fig. 2I,J; Table S4). We also found that, whereas Itga6 was localized at higher levels in retinal astrocyte processes and endfeet (Fig. 8E-G, filled arrowheads), integrin-α2 (upregulated in the *Apcdd1*$^{-/-}$ retina at P10; Fig. 2I; Table S4) did not colocalize to astrocyte processes and endfeet (Fig. 8B-D, unfilled arrowheads). These data are consistent with *in vitro* findings that Itga6b1 binds several laminin trimers, including laminin-211 (Nishiuchi et al., 2006). Quantification of the ratio of Itga6 over GFAP M.F.I. at P10 and P14 WT and *Apcdd1*$^{-/-}$ retinas showed a significant upregulation of Itga6 intensity in *Apcdd1*$^{-/-}$ retinal astrocytes at both P10 (~40%; Fig. 8L,Q) and P14 (~50%; Fig. 8H-Q) compared with WT astrocytes. These observations are consistent with a previous report that integrin expression is regulated by the presence of the cognate laminin ligands in the vBM (Gnanaguru et al., 2013). Itga6 expression was also increased in *Apcdd1*$^{-/-}$ compared with WT cerebellar astrocytes (Fig. S7G-L), similar to the retina.

To confirm whether astrocytic Itga6 regulates *GFAP* and *Aqp4* expression levels in response to laminin-211, we cultured cerebellar astrocytes on laminin-211 in the presence of Itga6-blocking antibodies or controls (heat-killed Itga6-blocking antibodies) (Fig. 8R-V). Blocking Itga6 binding to laminin-211 drastically reduced GFAP and Aqp4 expression levels in cultured astrocytes (Fig. 8T-V). Thus, astrocytic Itga6 (likely α6β1) is responsible for mediating interactions of astrocytes with Lama2 in the vBM and this interaction affects astrocyte maturation and polarization around blood vessels in the developing CNS.

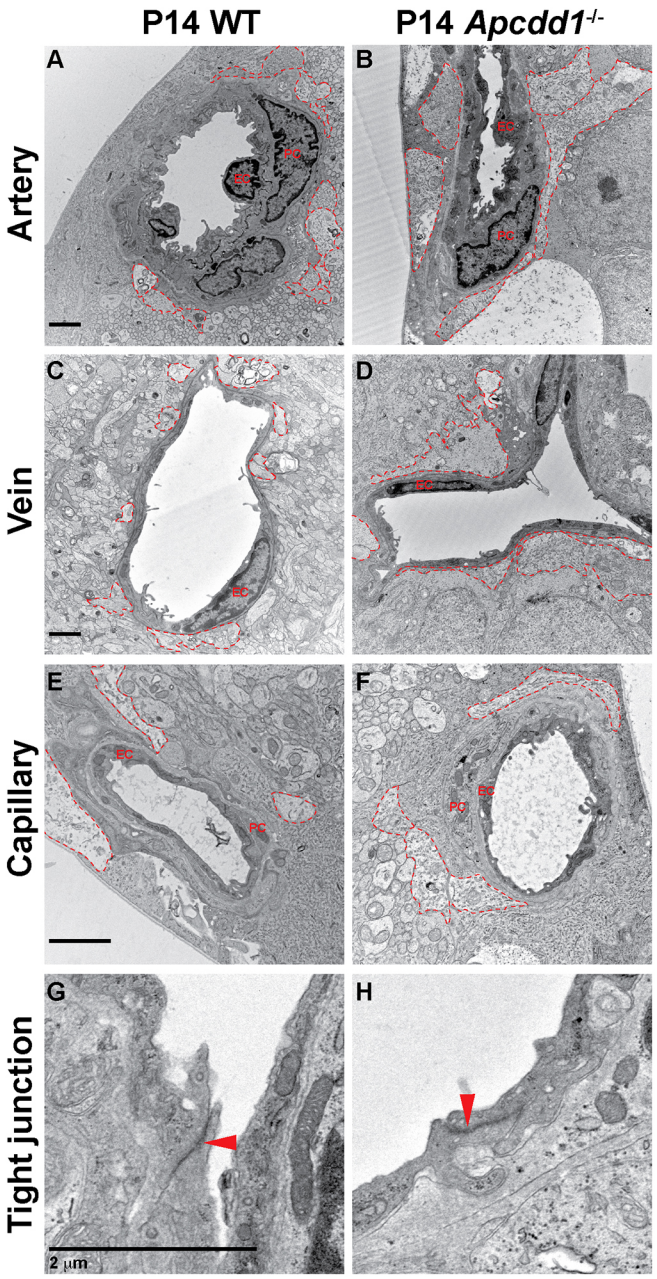

Fig. 7. *Apcdd1*$^{-/-}$ retinal vessels have more extensive astrocyte endfeet coverage at the electron microscopy level compared with wild type. (A-F) TEM analyses of astrocyte endfeet coverage (red outlines) around the WT (A,C,E) and *Apcdd1*$^{-/-}$ (B,D,F) retinal superficial blood vessels show more-extensive endfeet coverage of arteries and veins in *Apcdd1*$^{-/-}$ retinas. (G,H) Ultrastructural analysis of endothelial tight junctions (red arrowheads) shows no obvious difference between WT and *Apcdd1*$^{-/-}$ retinas.

DISCUSSION

Vascular basement membrane proteins, especially laminins and collagen IV, play a crucial role in maintaining BBB/BRB integrity (Armulik et al., 2010; Chen et al., 2013; Cottarelli et al., 2020; Gautam et al., 2016; Gnanaguru et al., 2013; Menezes et al., 2014; Sixt et al., 2001; Yao et al., 2014). The molecular mechanisms that regulate the expression and deposition of vBM components in the CNS remain elusive, although they may provide potential therapeutic strategies to restore neurovascular barrier integrity in CNS pathologies with impaired BBB/BRB.

Development (2022) 149, dev200610. doi:10.1242/dev.200610

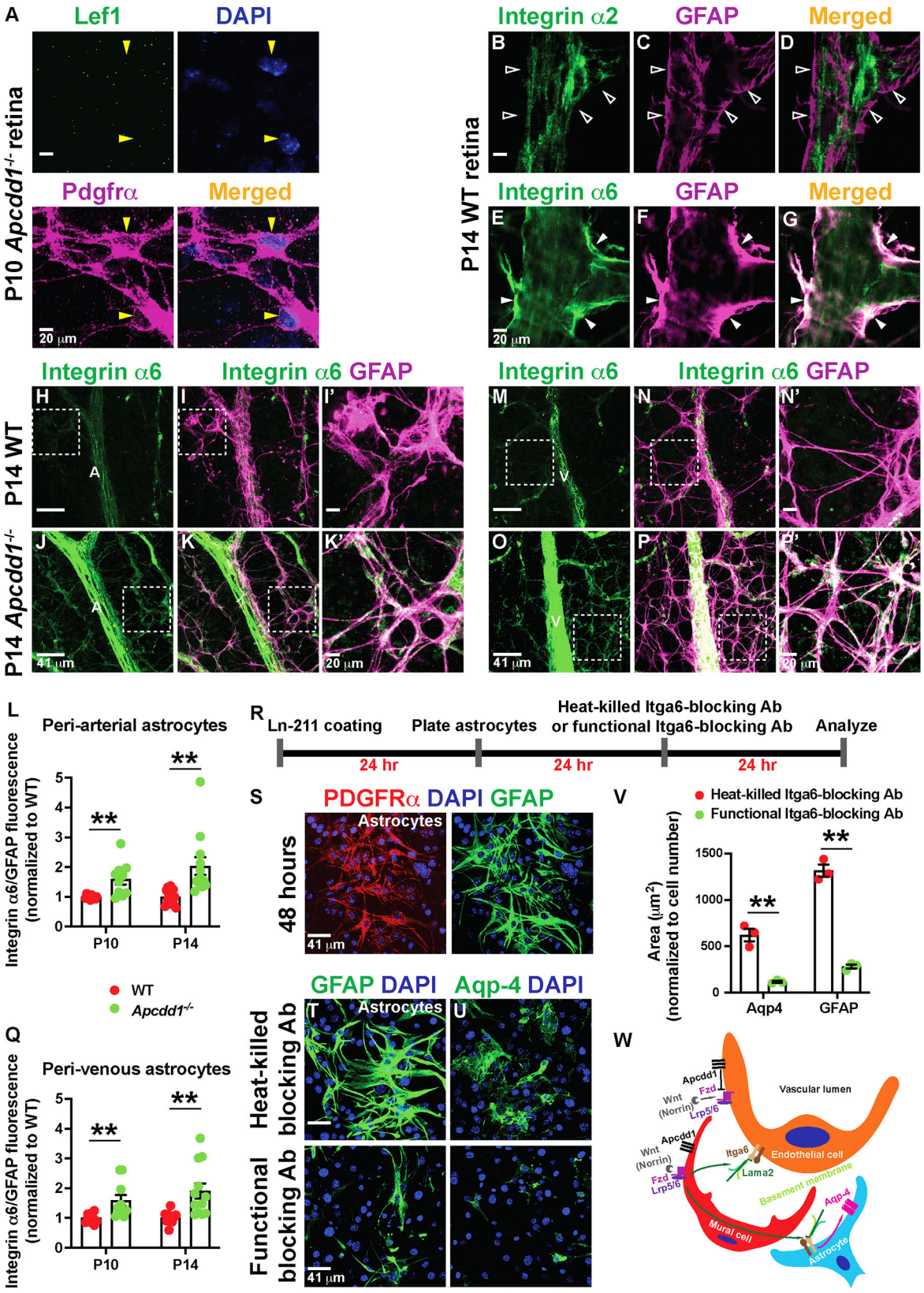

Fig. 8. See next page for legend.

Our study elucidates a missing link between the role of Wnt (Norrin)/β-catenin signaling in BBB/BRB maturation and the induction of vBM proteins. Previous studies addressing the role of Wnt/β-catenin pathway in the BBB/BRB formation primarily focused on ECs (Cottarelli et al., 2020; Daneman et al., 2009; Lengfeld et al., 2017; Liebner et al., 2008; Mazzoni et al., 2017; Wang et al., 2018, 2012; Ye et al., 2009; Zhou et al., 2014). To our knowledge, this is the first study to demonstrate that Wnt/β-catenin

Development (2022) 149, dev200610. doi:10.1242/dev.200610

Fig. 8. Astrocytic Itga6 expression is upregulated in *Apcdd1*$^{-/-}$ retinas. (A) P10 *Apcdd1*$^{-/-}$ retinal flat-mounts stained for Lef1, Pdgfrα and DAPI. Yellow arrowheads indicate Lef1^{-} astrocytes. (B-G) P14 WT retinal flat-mounts stained for either integrin-α2 (B-D) or Itga6 (E-G) and GFAP. Unfilled arrowheads indicate the lack of integrin-α2 expression in astrocytes. Filled arrowheads indicate Itga6 expression in astrocytes. (H-Q) P14 WT and *Apcdd1*$^{-/-}$ retinal flat-mounts stained for Itga6 and GFAP in arteries (H-K′) and veins (M-P′). A, artery; V, vein. Corresponding boxed areas are magnified in I′,K′,N′,P′. Ratio of Itga6/GFAP M.F.I. in peri-arterial (L) and perivenous (Q) astrocytes, normalized to WT average values (ten arteries from *n*=5 mice/group at P10 and 12 arteries from *n*=6 mice/group at P14). (R-U) Primary mouse brain astrocytes were cultured on laminin-211-coated plates in the presence of either Itga6-blocking antibodies (Abs) or heat-killed Itga6-blocking Abs (control), and stained for Pdgfrα, GFAP, Aqp4 and DAPI. (V) GFAP^{+} and Aqp4^{+} astrocyte area (*n*=3 independent experiments). (W) Proposed model by which mural Wnt/β-catenin signaling regulates Lama2 deposition to the vBM and NVU maturation (see Discussion). Data are mean±s.e.m., analyzed with two-tailed unpaired Student's *t*-test: ***P*<0.02.

signaling is activated in CNS mural cells and that Wnt/β-catenin signaling regulates Lama2 expression and deposition to the vBM and, thus, the maturation of astrocytes and BBB/BRB properties.

Although Wnt/β-catenin signaling activation in ECs during CNS development is well established (reviewed by Biswas et al., 2020), we found that CNS mural cells also have active Wnt/β-catenin signaling, albeit at a lower level compared with ECs. Our findings are consistent with single-cell RNA-seq studies that several pathway components, including receptors (e.g. *Fzd4* and *Lrp5*), downstream effectors (e.g. *Lef1*) and negative regulators (e.g. *Apcdd1* and *Axin2*), are expressed by P14 retinal and adult brain mural cells (He et al., 2018; Macosko et al., 2015; Vanlandewijck et al., 2018). In contrast, retinal astrocytes do not show active Wnt/β-catenin signaling. One possibility for why Wnt/β-catenin signaling is lower in CNS mural cells than in ECs is that negative regulators of the pathway may be expressed at higher levels in mural cells [e.g. *Axin2* or *Nkd2* mRNA levels are higher in adult brain or P14 retinal PCs than in ECs (He et al., 2018; Macosko et al., 2015; Vanlandewijck et al., 2018)]. These negative regulators may shut down Wnt/β-catenin pathway activation more rapidly in CNS mural cells compared with ECs.

Although vBM components, such as collagen IV and laminins, are important for maintaining BBB/BRB integrity (Baeten and Akassoglou, 2011; Chen et al., 2013; Cottarelli et al., 2020; Gautam et al., 2016; Gnanaguru et al., 2013; Gould et al., 2005; Menezes et al., 2014; Sixt et al., 2001; Yao et al., 2014), the signaling pathways that regulate their expression by NVU cells and deposition to vBM are unknown. We have previously shown that expression of Fgfbp1, a downstream effector of the Wnt/β-catenin signaling in ECs, regulates collagen IV deposition in the vBM (Cottarelli et al., 2020). Whether Wnt/β-catenin signaling may also regulate vBM deposition of laminins is unknown. Although astrocytes were thought traditionally to be the main NVU cell source of Lama2 expression and deposition to the vBM (Sixt et al., 2001), recent single-cell RNA-seq studies revealed that mural cells are the major source of *Lama2* transcripts in either adult brain or P14 retina (Armulik et al., 2010; He et al., 2018; Macosko et al., 2015; Menezes et al., 2014; Vanlandewijck et al., 2018). Using FISH or *Lama2*$^{lacZ/+}$ reporter mice, we confirmed that *Lama2* mRNA or vascular β-Gal colocalize predominantly with mural cells and partially with astrocytes. Lama2 is crucial to maintain BBB integrity (Menezes et al., 2014); our findings demonstrate that it is also essential for BRB integrity. We found reduced occludin expression in *Lama2*$^{-/-}$ retinal ECs, consistent with impaired paracellular BRB permeability, a phenotype opposite to the *Apcdd1*$^{-/-}$ retina (Mazzoni et al., 2017) in which Wnt/β-catenin signaling and Lama2 expression and deposition to the vBM are upregulated. Previous studies have shown that loss of Wnt/β-catenin signaling in retinal ECs reduces the expression of tight junction proteins (Wang et al., 2018, 2012). Thus, the expression and organization of EC tight junction proteins in the CNS appear to be regulated by at least two mechanisms: (1) Wnt/β-catenin signaling in ECs; and (2) laminin composition of the vBM.

Our findings indicate that Wnt/β-catenin activity in CNS mural cells is an upstream and positive regulator of Lama2 expression and deposition to the vBM. In *Apcdd1*$^{-/-}$ mice, in which Wnt/β-catenin signaling is upregulated, leading to precocious BRB maturation (Mazzoni et al., 2017), we found that *Lama2* mRNA expression is increased in mural cells, resulting in higher deposition of Lama2 to the vBM, as revealed by four independent approaches: (1) a bulk RNA-seq comparison between WT and *Apcdd1*$^{-/-}$ retinas; (2) FISH for *Lama2*; (3) western blot of retinal lysates; and (4) immunolabeling of retinas and cerebella for Lama2. Given that both ECs and mural cells express Apcdd1 and ECs do not produce Lama2, our findings suggest that Wnt/β-catenin signaling in mural cells facilitates Lama2 expression and deposition to the vBM in the developing CNS. Consistent with this hypothesis, pharmacological activation of Wnt/β-catenin signaling in primary brain PCs increases Lama2 production *in vitro*, but not in ECs or astrocytes. As only a subset of retinal PCs express *Apcdd1* mRNA compared with ECs (Fig. 2D), this may account for the modest effects on Lama2 expression and deposition in the vBM observed in *Apcdd1*$^{-/-}$ retinas, and no obvious effect on vBM thickness, as assessed by TEM.

It is possible that reciprocal signaling between ECs and mural cells is affected in the *Apcdd1*$^{-/-}$ retina, which could also affect Lama2 production by mural cells as a secondary effect. However, none of the transcripts for signaling pathways responsible for EC-mural cell interactions [e.g. *Tgfb*, *Tgfbr1*, *Smad2/3*, *Ang1* (*Angpt1*), *Ang2* (*Angpt2*), *Tie2* (Tek), *Jag1* or *Notch3*] were differentially expressed between *Apcdd1*$^{-/-}$ and WT retinas in our bulk RNA-seq analyses. Thus, the most plausible explanation is that Wnt/β-catenin activity in mural cells directly induces Lama2 expression and deposition to the vBM.

What are the effects of increased Lama2 deposition to the *Apcdd1*$^{-/-}$ retinal NVU? Our data demonstrate that *Apcdd1*$^{-/-}$ retinal astrocytes have increased expression of several maturity markers, including *Gfap* (Tao and Zhang, 2014) and *Aqp4* (Li et al., 2019) by P14. Aqp4 expression is lost from polarized astrocyte endfeet in several retinovascular disorders associated with BRB dysfunction, such as experimental autoimmune uveitis (Motulsky et al., 2010), and genetic ablation of *Aqp4* also leads to disrupted BRB integrity (Nicchia et al., 2004). Our findings are consistent with previous studies demonstrating that Aqp4 localization in glial endfeet is regulated by the BM composition (Hirrlinger et al., 2011; Menezes et al., 2014). Although GFAP upregulation could indicate reactive astrogliosis, other established reactive astrogliosis marker (Escartin et al., 2021) genes, with the exception of *Tspo*, were not upregulated in *Apcdd1*$^{-/-}$ retinas. *Tspo* is also expressed by other retinal cell types, such as Müller cells, horizontal cells, ECs, PCs, microglia and amacrine cells (Macosko et al., 2015). These findings suggest that *Apcdd1*$^{-/-}$ retinal astrocytes are not reactive, and support our interpretation that GFAP upregulation is indicative of maturation. *Itga6* expression was upregulated in *Apcdd1*$^{-/-}$ retinal astrocytes, as well as in ECs. Itga6 forms a dimer with β1 (Baeten and Akassoglou, 2011), an ECM receptor expressed in astrocytes, to bind various laminins, including laminin-211 (Menezes et al., 2014;

Development (2022) 149, dev200610. doi:10.1242/dev.200610

Nishiuchi et al., 2006). However, we cannot rule out the involvement of other integrins, such as α6β4, in this process.

Our findings led us to propose a previously unknown role for Wnt/β-catenin signaling in NVU and BRB/BBB maturation (Fig. 8W). Mural cells express components of the Wnt/β-catenin signaling pathway, such as Lrp5/6, Fzd, Apcdd1. The activation of Wnt/β-catenin signaling in retinal mural cells leads to the production and deposition of Lama2 to the vBM. Astrocytes also produce Lama2 chains, but do not have active Wnt/β-catenin signaling. Thus, the upregulation of Wnt/β-catenin signaling resulting from the loss of Apcdd1 increases Lama2 production only by mural cells. ECs and astrocytes express Itga6b1, a laminin receptor the expression of which is upregulated in response to increased Lama2 in the *Apcdd1*$^{-/-}$ vBM. We postulate that the increased binding of Itga6b1 to Lama2 in the vBM of *Apcdd1*$^{-/-}$ retinas and cerebella induces a precocious maturation of astrocytes, leading to precocious polarization of astrocyte endfeet around blood vessels reflected by the upregulation of Aqp4 around CNS blood vessels in *Apcdd1*$^{-/-}$ retinas. Consequently, these changes lead to precocious BBB/BRB maturation in the *Apcdd1*$^{-/-}$ retinas and cerebella. A limitation of our study is the lack of genetic evidence demonstrating that Wnt/β-catenin signaling in mural cells is required for Lama2 expression. Future studies, such as deletion of Wnt receptors or downstream effectors specifically from mural cells, will address this issue. Given that Wnt/β-catenin signaling in both ECs and mural cells regulates BBB/BRB integrity, this may be a target for pharmacological intervention in neurovascular diseases in which BBB/BRB integrity is compromised.

MATERIALS AND METHODS

Mice

All animal usage and protocols were approved by the Institutional Animal Care and Use Committee (IACUC) at Columbia University Irving Medical Center. Experimental procedures were optimized to minimize animal stress and the number of animals used for experiments. Both sexes (males and females) were used for experiments and analyses.

Apcdd1 mutant mice genotyping

The generation and validation of *Apcdd1*$^{-/-}$ mice (CD1 background) have been previously described (Mazzoni et al., 2017). These mice were bred as *Apcdd1*$^{+/-}$ and gave birth in Mendelian ratios. Age-matched littermate WT and *Apcdd1*$^{-/-}$ mice were used for experiments. PCR primers for the *Apcdd1* WT allele were: forward (5′-GAGTGTCCCCGACTCCGACTCT-3′); reverse (5′-ATGTGTTGAGTTATTCCCGGAAG-3′). PCR primers for the *Apcdd1* mutant allele were: forward (5′-GCCCATCTGGGATAGTACATGTG-3′); reverse (5′-CCTGGACTGAGGGCCATAGGTAAGAGG-3′).

Tcf/Lef::H2B-eGFP mice genotyping

The generation and validation of *Tcf/Lef*::H2B-eGFP transgenic mice (BL/6J background) have been previously described (Lengfeld et al., 2017). PCR primers for the *GFP* allele were: forward (5′-CCCTGAAGTT-CATCTGCACCAC-3′); reverse (5′-TTCTCGTTGGGGTCTTTGCTC-3′).

Lama2$^{lacZ/+}$ mice genotyping

Lama2$^{lacZ/+}$ mice [B6.129S1(Cg)-*Lama2*^{tm1Eeng}/J, RRID:IMSR_JAX:013786 (Kuang et al., 1998)] were obtained from the Jackson Laboratory. Breeding between *Lama2*$^{lacZ/+}$ mice resulted in young born in Mendelian ratios, and age-matched littermate WT, *Lama2*$^{lacZ/+}$ and *Lama2*$^{lacZ/lacZ}$ (*Lama2*$^{-/-}$) mice were used for experiments. PCR primers for the *Lama2* WT and mutant alleles were: forward (5′-ACTGCCCTTTCTCACCCACCCTT-3′); reverse (wild type: 5′-GTTGATGCGCTTGGGAC-3′; *lacZ*: 5′-CGACAGTATCGGCCTCAG-3′). *Lama2*$^{-/-}$ pups died around P14 as a result of complications associated with merosin (Lama2)-dependent congenital muscular dystrophy.

Primary vascular brain pericyte, astrocyte and endothelial cell cultures

Primary brain vascular PCs (iXCells Biotechnologies, 10MU-014), astrocytes (cerebellar: ScienCell, M1810-57) and ECs (Cell Biologics, C57-6023) were cultured in dishes coated with PDL (10 µg/ml) and collagen IV (20 µg/ml) and PCs were seeded onto the coated plates. Cells were cultured with PC (iXCells Biotechnologies, MD-0030), astrocyte (ScienCell, M1831) or endothelial (Cell Biologics, M1168) growth media. Media was changed every 48 h until the cells were 80% confluent. Next, the cells were detached with 0.25% trypsin and plated onto 24-well glass plates coated with PDL and collagen IV. Media were changed every 24 h. For Lama2 and Lef1 staining, CHIR99021 (1 µM; Selleck Chemicals, S1263), DMSO (control) or recombinant human Wnt3a (0.5 µg/ml; Thermo Fisher Scientific, 5036WN010) was added to the media after 24 h and repeated every 24 h for 2 days. The media were then aspirated, the cells were fixed with 2% paraformaldehyde (PFA) for 10 min and processed for immunohistochemistry. For Pdgfrα, GFAP and Aqp4 stainings of astrocytes, astrocytes were seeded onto plates coated with recombinant laminin-211 (40 µg/ml; BioLamina, LN211-0501). After 24 h, either active Itga6-blocking antibodies (Millipore Sigma, MAB1378, NKI-GoH3; 40 µg/ml) or heat-killed Itga6-blocking antibodies were added to the media, followed by a repeat application every 24 h for 2 days. Cells were blocked for 2 h at room temperature followed by primary antibody incubation (see below) overnight at 4°C. Following one PBS wash, cells were incubated with secondary antibodies (see below) for 4 h at room temperature. Cells were imaged using a ZEISS LSM700 confocal microscope and analyzed using Fiji software (National Institutes of Health).

Bulk RNA sequencing and assignment of putative cellular sources for differentially expressed transcripts

Total cellular RNA was extracted from P10 and P14 WT and *Apcdd1*$^{-/-}$ retinas using a QIAGEN RNeasy Mini Kit. Eight retinas from four pups were combined for each sample in each genotype. Concentrations of isolated RNA samples were ascertained using a NanoDrop Spectrophotometer (ND-100). RNA samples were sent to either the New York Genome Center (P10) or Genewiz (P14) for sequencing. cDNA libraries were prepared from RNA samples and sequenced to generate read counts for individual RNA species. Differential expression analyses were performed for these RNAs using the Bioconductor package DESeq2 in R. Cutoffs of the Benjamini–Hochberg adjusted *P*-values (padj) ≤ 0.05 and $|\log_2$ fold change$| \geq 0.5$ were used to identify statistically significant, differentially expressed genes. Putative cellular sources for differentially expressed transcripts between P10 or P14 *Apcdd1*$^{-/-}$ versus WT retinas were determined from the existing retinal single-cell RNA-seq gene expression database (https://singlecell.broadinstitute.org/single_cell/study/SCP301/c57b6-wild-type-p14-retina-by-drop-seq#study-summary) (Macosko et al., 2015). Genes were assigned to a specific cell type if they showed a mean level of expression in that particular cell type >0. Genes that were expressed in multiple retinal cell types in the database were assigned to all the cell types they were expressed in. Volcano plots for each gene category were constructed using the R software package and the top upregulated and downregulated genes as well as other specific genes of interest within each plot were identified (Tables S1-S5).

In vivo tracer injection

Mice were anesthetized using isoflurane and injected with 1% biocytin-5(and-6)-tetramethylrhodamine (biocytin-TMR; Thermo Fisher Scientific, T12921). After 30 min in circulation, mice were re-anesthetized and perfused with 1× phosphate buffer saline (PBS) via the cardiac route. Retinas and livers were isolated and fixed in 4% PFA for 2 h before immunostaining with FITC-conjugated lectin. Given that blood vessels in the liver do not have a barrier, biocytin-TMR fluorescence in the livers of corresponding animals was used as internal controls for the measurement of biocytin-TMR fluorescence in the retina, as previously described (Lengfeld et al., 2017; Mazzoni et al., 2017).

Development (2022) 149, dev200610. doi:10.1242/dev.200610

Immunofluorescence

Unless otherwise specified, isolated tissues (retina, brain and liver) were fixed in 4% PFA for 2 h for immunostaining. The exceptions were retinal flat-mount staining for laminin chains and integrin subunits, whereby retinas were fixed for 10 min in 2% PFA. For retinal flat-mounts, tissues were washed once with PBS following PFA fixation and blocked overnight in blocking buffer (5% goat or donkey serum, 0.3% Triton X-100 in 1× PBS) at 4°C. Samples were then incubated with primary antibodies in antibody-diluting solution (5% goat or donkey serum; 0.01% Triton X-100 in 1× PBS) for 48 h at 4°C, washed and then incubated with secondary antibodies for 24 h. For radial section staining, samples were washed in 1× PBS, cryoprotected in 30% sucrose overnight, embedded in optimal cutting temperature compound (Tissue-Tek) and sectioned at a thickness of 12 µm. Tissue sections were blocked for 2 h at room temperature followed by primary antibody incubation overnight at 4°C. Following 1× PBS washes, sections were incubated with secondary antibodies for 4 h at room temperature. Samples were imaged at room temperature using a ZEISS LSM700 confocal microscope [20× air (objective Plan-Apochromat 20×/0.8 M27; numerical aperture: 0.8) or 40× water (objective C-Apochromat 40×/1.2 W autocorr M27; numerical aperture: 1.2) objectives; ZEN image acquisition software] and analyzed using Fiji software as previously described (Mazzoni et al., 2017).

Antibodies used in immunofluorescence

Primary antibodies used were: rat anti-CD31 (1:250; BD Biosciences, 553370, RRID: AB_394816), rabbit anti-CD31 (1:250; Abcam, AB28364, RRID: AB_726362), goat anti-Pdgfrβ (1:200; R&D Systems, AF1042, RRID: AB_2162633), FITC-conjugated rabbit anti-LEF1 (1:100; Cell Signaling Technology, 2230s, RRID: AB_823558), rabbit anti-GFP (1:500; Thermo Fisher Scientific, A11122, RRID: AB_221569), rabbit anti-NG2 (1:250; Millipore, AB5320, RRID: AB_11213678), goat anti-β-Gal (1:250; Abcam, AB12081, RRID: AB_725684), rat anti-Lama2 (1:200; Abcam, AB11576, RRID: AB_298180), rat anti-laminin β1 (1:200; Abcam, AB44941, RRID: AB_775971), rabbit anti-laminin β2 (1:1000; a gift from Dr William J. Brunken, SUNY Upstate Medical University, Syracuse, NY, USA), rabbit anti-GFAP (1:1000; Millipore, AB5804, RRID: AB_2109645), rat anti-Pdgfrα (1:100; BD Biosciences, 558774, RRID: AB_397117), rabbit anti-Aqp4 (1:250; Sigma-Aldrich, A5971, RRID: AB_258270), rat anti-Itga6 (1:100; Millipore, MAB1982, RRID: AB_2128296), rat anti-human ITGA6 (ITGA6-blocking antibody: clone NKI-GoH3; Millipore, MAB1378, RRID: AB_2128317) and FITC-conjugated mouse anti-integrin-α2 (1:100; Santa-Cruz Biotechnology, sc-74466, RRID: AB_1124939). Secondary antibodies used were: goat anti-rat Alexa Fluor 594 (A11007), goat anti-rabbit Alexa Fluor 594 (A11012), goat anti-rat Alexa Fluor 488 (A11006), goat anti-rabbit Alexa Fluor 488 (A11034), donkey anti-rat Alexa Fluor 594 (A21209), donkey anti-rabbit Alexa Fluor 594 (A32754), donkey anti-rat Alexa Fluor 488 (A21208), donkey anti-rabbit Alexa Fluor 488 (A21206), donkey anti-rat Alexa Fluor 647 (A48272), donkey anti-rabbit Alexa Fluor 647 (A32795), donkey anti-goat Alexa Fluor 594 (A32758) and donkey anti-goat Alexa Fluor 488 (A11055) (all 1:250; Thermo Fisher Scientific). Other reagents used were fluorescein *Griffonia simplicifolia* lectin I (isolectin B4; 1:250; Vector Laboratories; FL-1201, RRID: AB_2314663).

RNA fluorescence *in situ* hybridization

Antisense mRNA probe for *Lama2* was prepared using TOM6004-MGC premier ORF clone for *Lama2* (Transomic Technologies; clone ID: BC172647, Accession: BC172647). The preparation and validation of antisense mRNA probes for full-length *Apcdd1* was as previously described (Mazzoni et al., 2017). FISH using these probes were performed as previously described (Mazzoni et al., 2017). In case of FISH combined with immunolabeling with EC, mural cell and astrocyte markers, the samples were immunostained for caveolin 1 (1:500; Abcam, AB18199, RRID: AB_444314), Pdgfrβ or NG2, and GFAP, respectively, after *in situ* hybridization for *Apcdd1* or *Lama2* mRNAs. The samples were imaged using a ZEISS LSM700 confocal microscope and analyzed using Fiji software.

Western blotting

Retinas were collected from mice after perfusion with PBS. Eight retinas from four mice were combined for each sample. Collected tissue was homogenized in lysis buffer containing protease and phosphatase inhibitors using a Dounce homogenizer followed by sonication. Protein levels in P10, P14 and P18 retinas were measured by fluorescent western blot analysis [4-15% or 7.5% Mini-PROTEAN TGX gels (Bio-Rad)] and quantitation was performed using the LICOR system, as previously described (Mazzoni et al., 2017). Western blot analysis used the following primary antibodies: rat anti-Lama2 (1:200; Abcam, AB11576, RRID: AB_298180), rabbit anti-laminin (1:2500; Sigma-Aldrich, L9393, RRID: AB_477163; primarily recognizes Lama1), rabbit anti-aqp4 (1:250; Sigma-Aldrich, A5971, RRID: AB_258270) and anti-β-actin (1:10,000; Novus Biologicals, NB600-501, RRID: AB_10077656). IRDyes 680 and 800 (1:20,000; LI-COR) were used as secondary antibodies. Fluorescent quantification of protein levels was performed using the Odyssey SA infrared imaging system. Values are displayed as protein levels corrected with β-actin and normalized to WT control values.

Transmission electron microscopy

Animals were anesthetized as described above, followed by perfusion with fixative solution (4% PFA and 2% glutaraldehyde in 0.1 M sodium cacodylate) for 5 min at 4 ml/min. After perfusion, eyeballs were dissected and stored in fixative solution overnight at 4°C, followed by washing with buffer (0.1 M sodium cacodylate) and water. The corneas and lenses were removed from the eyeballs and the eyecups were stored in the fixative solution until further processing. Samples were treated with 1% reduced osmium tetroxide and dehydrated in an ethanol series, followed by treatment with acetonitrile. Samples were then embedded in LX112 resin (Ladd Research Industries) and sectioned. Sections were contrasted with uranyl acetate and lead citrate for imaging in JEOL JEM-1400 TEM equipped with a Veleta (EMSIS, GmbH) CCD camera in the Microscopy and Image Analysis Core Facility, Weill Cornell Medicine (New York, NY, USA).

Image acquisition and analysis

For retinal flat-mounts, each measurement was made in at least three quadrants per sample. For sections, at least three sections were imaged per sample. In each case, multiple representative images were acquired and averaged. To measure the number of Lef1$^+$ and nGFP$^+$ mural cells (Fig. 1), the area positive for Pdgfrβ was measured from each image in Fiji software using signal masking and the number of Lef1$^+$ and nGFP$^+$ nuclei within that Pdgfrβ$^+$ area was quantified and normalized to unit area. To measure *Apcdd1* expression in ECs and mural cells (Fig. 2), the number of Apcdd1$^+$/Pdgfrβ$^+$ or Apcdd1$^+$/Cav1$^+$ cells was quantified and presented as the percentage of total Pdgfrβ$^+$ or Cav1$^+$ cells, respectively. To measure *Lama2* mRNA expression in mural cells (Fig. 3), M.F.I. of *Lama2* puncta in individual mural cells were calculated with histogram analysis in Fiji software. To measure the deposition of laminins to the vBM (Fig. 3; Figs S3, S5), M.F.I. ratios (laminin:CD31) in individual vessel segments were calculated with histogram analysis in Fiji software. Data were presented as values normalized to the WT average values. To measure Lef1 expression *in vitro* (Fig. S4), the number of Lef1$^+$ nuclei was quantified as the percentage of total nuclei. To measure laminin deposition *in vitro* (Fig. S4), laminin M.F.I. was quantified from each image and normalized to the number of total nuclei. The intensity of biocytin-TMR outside of retinal vessels (tracer leakage; Fig. 4) was measured as previously described (Mazzoni et al., 2017). Biocytin-TMR signal intensities in the retina and cerebella were normalized to those of livers. To measure the relative expression of GFAP (Fig. 5), the M.F.I. were calculated for each field and data were presented as values normalized to the WT. To measure Aqp4$^+$ astrocyte endfeet coverage of arteries and veins (Fig. 5), the percentage of total vessel length surrounded by Aqp4$^+$ astrocyte endfeet in individual arterial and venous segments was calculated. To measure astrocytic expression of Itga6 (Fig. 6), M.F.I. ratios (Itga6/Gfap) in each field were calculated. Data were presented as values normalized to the WT average values.

Statistical analyses

Samples from 3-7 different animals (for *in vivo* experiments) and three or four separate experiments (for *in vitro* experiments) were used for statistical analysis. To test for the statistical significance of any differences, either one-way ANOVA or two-tailed unpaired Student's *t*-tests were performed. $P<0.05$ was considered statistically significant.

Acknowledgements
TEM (Microscopy and Image Analysis Core Facility, Weill Cornell Medicine) was supported by an NIH Shared Instrumentation Grant (S10RR027699).

Competing interests
The authors declare no competing or financial interests.

Author contributions
Conceptualization: S.B., T.C., D.A.; Methodology: S.B., D.A.; Software: S.S., N.P.G.; Validation: S.B.; Formal analysis: S.B., S.S., N.P.G., P.A., M.W.; Investigation: S.B., S.S., N.P.G.; Resources: W.J.B., D.A.; Data curation: S.B., S.S., N.P.G., P.A., M.W.; Writing - original draft: S.B., D.A.; Writing - review & editing: S.B., S.S., N.P.T., W.J.B., T.C., D.A.; Visualization: S.B.; Supervision: D.A.; Project administration: D.A.; Funding acquisition: N.P.T., W.J.B., D.A.

Funding
S.B., S.S., T.C. and D.A. are supported by grants from the National Institute of Mental Health (R01 MH112849), National Institute of Neurological Disorders and Stroke (R01 NS107344; R21 NS118891), the National Multiple Sclerosis Society (RG-1901-33218) and the Fondation Leducq (15CDV-02). W.J.B. is supported by grants from the National Eye Institute (R01-Ey12676) and in part by funds from an unrestricted grant from Research to Prevent Blindness to the Department of Ophthalmology and Visual Sciences, Upstate Medical University. N.P.G. and N.P.T. are supported by a grant from the National Institute of General Medical Sciences (R35GM131905). Deposited in PMC for release after 12 months.

Peer review history
The peer review history is available online at https://journals.biologists.com/dev/lookup/doi/10.1242/dev.200610.reviewer-comments.pdf.

References

Armulik, A., Genove, G., Mae, M., Nisancioglu, M. H., Wallgard, E., Niaudet, C., He, L., Norlin, J., Lindblom, P., Strittmatter, K. et al. (2010). Pericytes regulate the blood-brain barrier. *Nature* **468**, 557-561. doi:10.1038/nature09522

Baeten, K. M. and Akassoglou, K. (2011). Extracellular matrix and matrix receptors in blood-brain barrier formation and stroke. *Dev. Neurobiol.* **71**, 1018-1039. doi:10.1002/dneu.20954

Biswas, S., Watters, J., Bachay, G., Varshney, S., Hunter, D. D., Hu, H. and Brunken, W. J. (2018). Laminin-dystroglycan signaling regulates retinal arteriogenesis. *FASEB J.* **32**, 6261-6273. doi:10.1096/fj.201800232R

Biswas, S., Cottarelli, A. and Agalliu, D. (2020). Neuronal and glial regulation of CNS angiogenesis and barriergenesis. *Development* **147**, dev182279. doi:10.1242/dev.182279

Chen, J., Stahl, A., Krah, N. M., Seaward, M. R., Joyal, J.-S., Juan, A. M., Hatton, C. J., Aderman, C. M., Dennison, R. J., Willett, K. L. et al. (2012). Retinal expression of Wnt-pathway mediated genes in low-density lipoprotein receptor-related protein 5 (Lrp5) knockout mice. *PLoS One* **7**, e30203. doi:10.1371/journal.pone.0030203

Chen, Z.-L., Yao, Y., Norris, E. H., Kruyer, A., Jno-Charles, O., Akhmerov, A. and Strickland, S. (2013). Ablation of astrocytic laminin impairs vascular smooth muscle cell function and leads to hemorrhagic stroke. *J. Cell Biol.* **202**, 381-395. doi:10.1083/jcb.201212032

Cottarelli, A., Corada, M., Beznoussenko, G. V., Mironov, A. A., Globisch, M. A., Biswas, S., Huang, H., Dimberg, A., Magnusson, P. U., Agalliu, D. et al. (2020). Fgfbp1 promotes blood-brain barrier development by regulating collagen IV deposition and maintaining Wnt/β-catenin signaling. *Development* **147**, dev185140. doi:10.1242/dev.185140

Daneman, R., Agalliu, D., Zhou, L., Kuhnert, F., Kuo, C. J. and Barres, B. A. (2009). Wnt/β-catenin signaling is required for CNS, but not non-CNS, angiogenesis. *Proc. Natl. Acad. Sci. USA* **106**, 641-646. doi:10.1073/pnas.0805165106

Díaz-Coranguez, M., Ramos, C. and Antonetti, D. A. (2017). The inner blood-retinal barrier: Cellular basis and development. *Vision Res.* **139**, 123-137. doi:10.1016/j.visres.2017.05.009

Durbeej, M. (2010). Laminins. *Cell Tissue Res.* **339**, 259-268. doi:10.1007/s00441-009-0838-2

Escartin, C., Galea, E., Lakatos, A., O'Callaghan, J. P., Petzold, G. C., Serrano-Pozo, A., Steinhauser, C., Volterra, A., Carmignoto, G., Agarwal, A. et al. (2021). Reactive astrocyte nomenclature, definitions, and future directions. *Nat. Neurosci.* **24**, 312-325. doi:10.1038/s41593-020-00783-4

Fancy, S. P., Harrington, E. P., Baranzini, S. E., Silbereis, J. C., Shiow, L. R., Yuen, T. J., Huang, E. J., Lomvardas, S. and Rowitch, D. H. (2014). Parallel states of pathological Wnt signaling in neonatal brain injury and colon cancer. *Nat. Neurosci.* **17**, 506-512. doi:10.1038/nn.3676

Ferrer-Vaquer, A., Piliszek, A., Tian, G., Aho, R. J., Dufort, D. and Hadjantonakis, A. K. (2010). A sensitive and bright single-cell resolution live imaging reporter of Wnt/ß-catenin signaling in the mouse. *BMC Dev. Biol.* **10**, 121. doi:10.1186/1471-213X-10-121

Gautam, J., Zhang, X. and Yao, Y. (2016). The role of pericytic laminin in blood brain barrier integrity maintenance. *Sci. Rep.* **6**, 36450. doi:10.1038/srep36450

Gnanaguru, G., Bachay, G., Biswas, S., Pinzón-Duarte, G., Hunter, D. D. and Brunken, W. J. (2013). Laminins containing the β2 and γ3 chains regulate astrocyte migration and angiogenesis in the retina. *Development* **140**, 2050-2060. doi:10.1242/dev.087817

Gould, D. B., Phalan, F. C., Breedveld, G. J., van Mil, S. E., Smith, R. S., Schimenti, J. C., Aguglia, U., van der Knaap, M. S., Heutink, P. and John, S. W. (2005). Mutations in Col4a1 cause perinatal cerebral hemorrhage and porencephaly. *Science* **308**, 1167-1171. doi:10.1126/science.1109418

He, L., Vanlandewijck, M., Mae, M. A., Andrae, J., Ando, K., Del Gaudio, F., Nahar, K., Lebouvier, T., Laviña, B., Gouveia, L. et al. (2018). Single-cell RNA sequencing of mouse brain and lung vascular and vessel-associated cell types. *Sci. Data* **5**, 180160. doi:10.1038/sdata.2018.160

Hirrlinger, P. G., Pannicke, T., Winkler, U., Claudepierre, T., Varshney, S., Schulze, C., Reichenbach, A., Brunken, W. J. and Hirrlinger, J. (2011). Genetic deletion of laminin isoforms β2 and γ3 induces a reduction in Kir4.1 and aquaporin-4 expression and function in the retina. *PLoS One* **6**, e16106. doi:10.1371/journal.pone.0016106

Iadecola, C. (2017). The neurovascular unit coming of age: a journey through neurovascular coupling in health and disease. *Neuron* **96**, 17-42. doi:10.1016/j.neuron.2017.07.030

Iandiev, I., Biedermann, B., Bringmann, A., Reichel, M. B., Reichenbach, A. and Pannicke, T. (2006). Atypical gliosis in Muller cells of the slowly degenerating rds mutant mouse retina. *Exp. Eye Res.* **82**, 449-457. doi:10.1016/j.exer.2005.07.018

Junge, H. J., Yang, S., Burton, J. B., Paes, K., Shu, X., French, D. M., Costa, M., Rice, D. S. and Ye, W. (2009). TSPAN12 regulates retinal vascular development by promoting Norrin- but not Wnt-induced FZD4/β-catenin signaling. *Cell* **139**, 299-311. doi:10.1016/j.cell.2009.07.048

Kuang, W., Xu, H., Vachon, P. H., Liu, L., Loechel, F., Wewer, U. M. and Engvall, E. (1998). Merosin-deficient congenital muscular dystrophy. Partial genetic correction in two mouse models. *J. Clin. Invest.* **102**, 844-852. doi:10.1172/JCI3705

Lengfeld, J. E., Lutz, S. E., Smith, J. R., Diaconu, C., Scott, C., Kofman, S. B., Choi, C., Walsh, C. M., Raine, C. S., Agalliu, I. et al. (2017). Endothelial Wnt/β-catenin signaling reduces immune cell infiltration in multiple sclerosis. *Proc. Natl. Acad. Sci. USA* **114**, E1168-E1177. doi:10.1073/pnas.1609905114

Li, J., Khankan, R. R., Caneda, C., Godoy, M. I., Haney, M. S., Krawczyk, M. C., Bassik, M. C., Sloan, S. A. and Zhang, Y. (2019). Astrocyte-to-astrocyte contact and a positive feedback loop of growth factor signaling regulate astrocyte maturation. *Glia* **67**, 1571-1597. doi:10.1002/glia.23630

Liebner, S., Corada, M., Bangsow, T., Babbage, J., Taddei, A., Czupalla, C. J., Reis, M., Felici, A., Wolburg, H., Fruttiger, M. et al. (2008). Wnt/β-catenin signaling controls development of the blood-brain barrier. *J. Cell Biol.* **183**, 409-417. doi:10.1083/jcb.200806024

Liebner, S., Dijkhuizen, R. M., Reiss, Y., Plate, K. H., Agalliu, D. and Constantin, G. (2018). Functional morphology of the blood-brain barrier in health and disease. *Acta Neuropathol.* **135**, 311-336. doi:10.1007/s00401-018-1815-1

Luhmann, U. F., Lin, J., Acar, N., Lammel, S., Feil, S., Grimm, C., Seeliger, M. W., Hammes, H. P. and Berger, W. (2005). Role of the Norrie disease pseudoglioma gene in sprouting angiogenesis during development of the retinal vasculature. *Invest. Ophthalmol. Vis. Sci.* **46**, 3372-3382. doi:10.1167/iovs.05-0174

Macosko, E. Z., Basu, A., Satija, R., Nemesh, J., Shekhar, K., Goldman, M., Tirosh, I., Bialas, A. R., Kamitaki, N., Martersteck, E. M. et al. (2015). Highly parallel genome-wide expression profiling of individual cells using nanoliter droplets. *Cell* **161**, 1202-1214. doi:10.1016/j.cell.2015.05.002

Mazzoni, J., Smith, J. R., Shahriar, S., Cutforth, T., Ceja, B. and Agalliu, D. (2017). The Wnt inhibitor Apcdd1 coordinates vascular remodeling and barrier maturation of retinal blood vessels. *Neuron* **96**, 1055-1069.e6. doi:10.1016/j.neuron.2017.10.025

Menezes, M. J., McClenahan, F. K., Leiton, C. V., Aranmolate, A., Shan, X. and Colognato, H. (2014). The extracellular matrix protein laminin alpha2 regulates the maturation and function of the blood-brain barrier. *J. Neurosci.* **34**, 15260-15280. doi:10.1523/JNEUROSCI.3678-13.2014

Motulsky, E., Koch, P., Janssens, S., Lienart, M., Vanbellinghen, A. M., Bolaky, N., Chan, C. C., Caspers, L., Martin-Martinez, M. D., Xu, H. et al. (2010). Aquaporin expression in blood-retinal barrier cells during experimental autoimmune uveitis. *Mol. Vis.* **16**, 602-610.

Nicchia, G. P., Nico, B., Camassa, L. M., Mola, M. G., Loh, N., Dermietzel, R., Spray, D. C., Svelto, M. and Frigeri, A. (2004). The role of aquaporin-4 in the blood-brain barrier development and integrity: studies in animal and cell culture models. *Neuroscience* **129**, 935-944. doi:10.1016/j.neuroscience.2004.07.055

Nirwane, A. and Yao, Y. (2018). Laminins and their receptors in the CNS. *Biol. Rev. Camb. Philos. Soc.* [Epub ahead of print]

Nishiuchi, R., Takagi, J., Hayashi, M., Ido, H., Yagi, Y., Sanzen, N., Tsuji, T., Yamada, M. and Sekiguchi, K. (2006). Ligand-binding specificities of laminin-binding integrins: a comprehensive survey of laminin-integrin

interactions using recombinant α3β1, α6β1, α7β1 and α6β4 integrins. *Matrix Biol.* **25**, 189-197. doi:10.1016/j.matbio.2005.12.001

Patarroyo, M., Tryggvason, K. and Virtanen, I. (2002). Laminin isoforms in tumor invasion, angiogenesis and metastasis. *Semin. Cancer Biol.* **12**, 197-207. doi:10.1016/S1044-579X(02)00023-8

Paulus, W., Baur, I., Schuppan, D. and Roggendorf, W. (1993). Characterization of integrin receptors in normal and neoplastic human brain. *Am. J. Pathol.* **143**, 154-163.

Shimomura, Y., Agalliu, D., Vonica, A., Luria, V., Wajid, M., Baumer, A., Belli, S., Petukhova, L., Schinzel, A., Brivanlou, A. H. et al. (2010). APCDD1 is a novel Wnt inhibitor mutated in hereditary hypotrichosis simplex. *Nature* **464**, 1043-1047. doi:10.1038/nature08875

Siegenthaler, J. A., Choe, Y., Patterson, K. P., Hsieh, I., Li, D., Jaminet, S. C., Daneman, R., Kume, T., Huang, E. J. and Pleasure, S. J. (2013). Foxc1 is required by pericytes during fetal brain angiogenesis. *Biol. Open* **2**, 647-659. doi:10.1242/bio.20135009

Sixt, M., Engelhardt, B., Pausch, F., Hallmann, R., Wendler, O. and Sorokin, L. M. (2001). Endothelial cell laminin isoforms, laminins 8 and 10, play decisive roles in T cell recruitment across the blood-brain barrier in experimental autoimmune encephalomyelitis. *J. Cell Biol.* **153**, 933-946. doi:10.1083/jcb.153.5.933

Stenman, J. M., Rajagopal, J., Carroll, T. J., Ishibashi, M., McMahon, J. and McMahon, A. P. (2008). Canonical Wnt signaling regulates organ-specific assembly and differentiation of CNS vasculature. *Science* **322**, 1247-1250. doi:10.1126/science.1164594

Tao, C. and Zhang, X. (2014). Development of astrocytes in the vertebrate eye. *Dev. Dyn.* **243**, 1501-1510. doi:10.1002/dvdy.24190

Tran, F. H. and Zheng, J. J. (2017). Modulating the wnt signaling pathway with small molecules. *Protein Sci.* **26**, 650-661. doi:10.1002/pro.3122

Vanlandewijck, M., He, L., Mae, M. A., Andrae, J., Ando, K., Del Gaudio, F., Nahar, K., Lebouvier, T., Laviña, B., Gouveia, L. et al. (2018). A molecular atlas of cell types and zonation in the brain vasculature. *Nature* **554**, 475-480. doi:10.1038/nature25739

Wang, Y., Rattner, A., Zhou, Y., Williams, J., Smallwood, P. M. and Nathans, J. (2012). Norrin/Frizzled4 signaling in retinal vascular development and blood brain barrier plasticity. *Cell* **151**, 1332-1344. doi:10.1016/j.cell.2012.10.042

Wang, Y., Cho, C., Williams, J., Smallwood, P. M., Zhang, C., Junge, H. J. and Nathans, J. (2018). Interplay of the Norrin and Wnt7a/Wnt7b signaling systems in blood-brain barrier and blood-retina barrier development and maintenance. *Proc. Natl. Acad. Sci. USA* **115**, E11827-E11836. doi:10.1073/pnas.1813217115

Xia, C. H., Yablonka-Reuveni, Z. and Gong, X. (2010). LRP5 is required for vascular development in deeper layers of the retina. *PLoS One* **5**, e11676. doi:10.1371/journal.pone.0011676

Xu, Q., Wang, Y., Dabdoub, A., Smallwood, P. M., Williams, J., Woods, C., Kelley, M. W., Jiang, L., Tasman, W., Zhang, K. et al. (2004). Vascular development in the retina and inner ear: control by Norrin and Frizzled-4, a high-affinity ligand-receptor pair. *Cell* **116**, 883-895. doi:10.1016/S0092-8674(04)00216-8

Yao, Y., Chen, Z. L., Norris, E. H. and Strickland, S. (2014). Astrocytic laminin regulates pericyte differentiation and maintains blood brain barrier integrity. *Nat. Commun.* **5**, 3413. doi:10.1038/ncomms4413

Ye, X., Wang, Y., Cahill, H., Yu, M., Badea, T. C., Smallwood, P. M., Peachey, N. S. and Nathans, J. (2009). Norrin, frizzled-4, and Lrp5 signaling in endothelial cells controls a genetic program for retinal vascularization. *Cell* **139**, 285-298. doi:10.1016/j.cell.2009.07.047

Zhou, Y. and Nathans, J. (2014). Gpr124 controls CNS angiogenesis and blood-brain barrier integrity by promoting ligand-specific canonical Wnt signaling. *Dev. Cell* **31**, 248-256. doi:10.1016/j.devcel.2014.08.018

Zhou, Y., Wang, Y., Tischfield, M., Williams, J., Smallwood, P. M., Rattner, A., Taketo, M. M. and Nathans, J. (2014). Canonical WNT signaling components in vascular development and barrier formation. *J. Clin. Invest.* **124**, 3825-3846. doi:10.1172/JCI76431

Zuercher, J., Fritzsche, M., Feil, S., Mohn, L. and Berger, W. (2012). Norrin stimulates cell proliferation in the superficial retinal vascular plexus and is pivotal for the recruitment of mural cells. *Hum. Mol. Genet.* **21**, 2619-2630. doi:10.1093/hmg/dds087

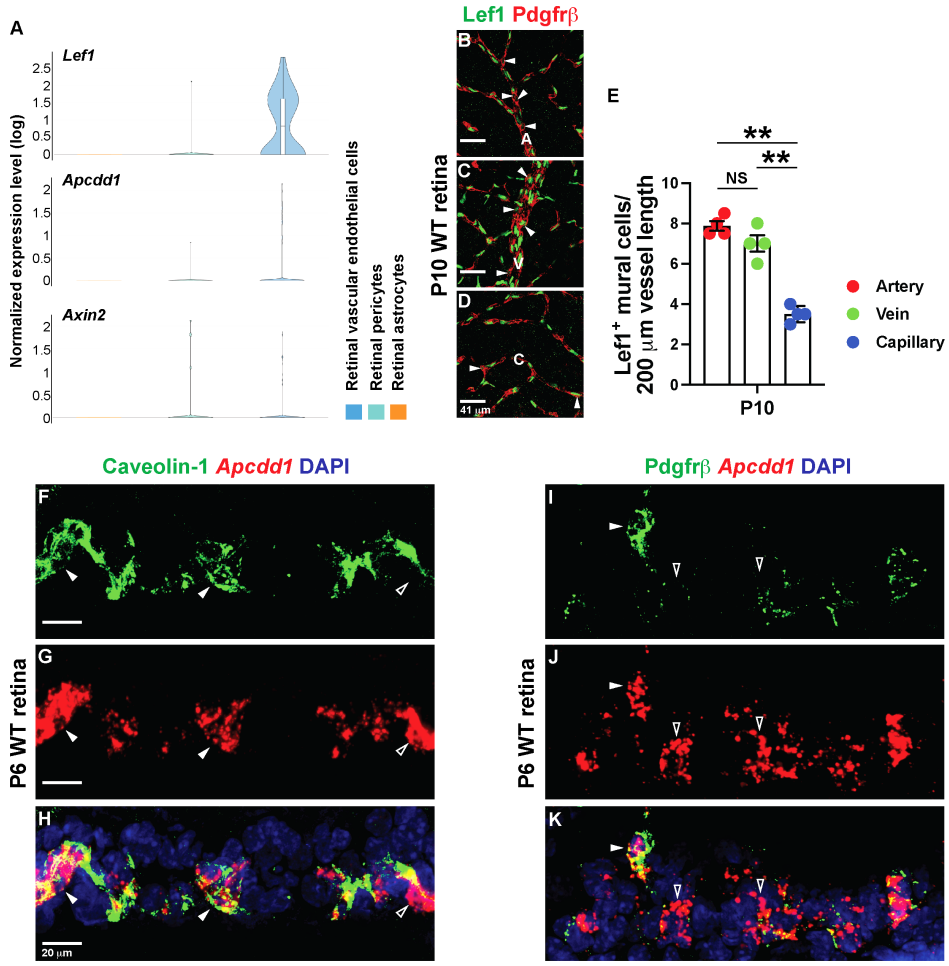

Fig. S1 (related to Figs. 1, 2, 3). Wnt/β-catenin signaling is activated in retinal ECs and mural cells, but not in astrocytes. A) Analyses of a P14 WT retinal single cell RNAseq database (see Results and Materials and Methods) to explore expression profiles of downstream Wnt/β-catenin targets (*Lef1*, *Apcdd1*, *Axin2*) in endothelial cells (ECs), pericytes (PCs) and astrocytes. **B-E)** P10 WT retinal flat-mounts were stained for Lef1 and Pdgfrβ (A= artery, V= vein, C= capillary). Solid arrowheads point to Lef1$^+$ mural cells. Dotted bar graph shows number of Lef1$^+$ mural cells in unit length for each vessel type (n=4 animals). **F-K)** Fluorescence *in situ* hybridization of P10 WT retinal sections with antisense probe against *Apcdd1* mRNA followed by immunostaining for Caveolin-1 or Pdgfrβ proteins. Solid arrowheads and empty arrowheads point to localization of *Apcdd1* mRNA inside and outside the corresponding cells marker, respectively. Student's t-test: **p<0.02, NS: not significant. Graphs show mean +/- SEM. Scale bars: B-D = 41 μm.

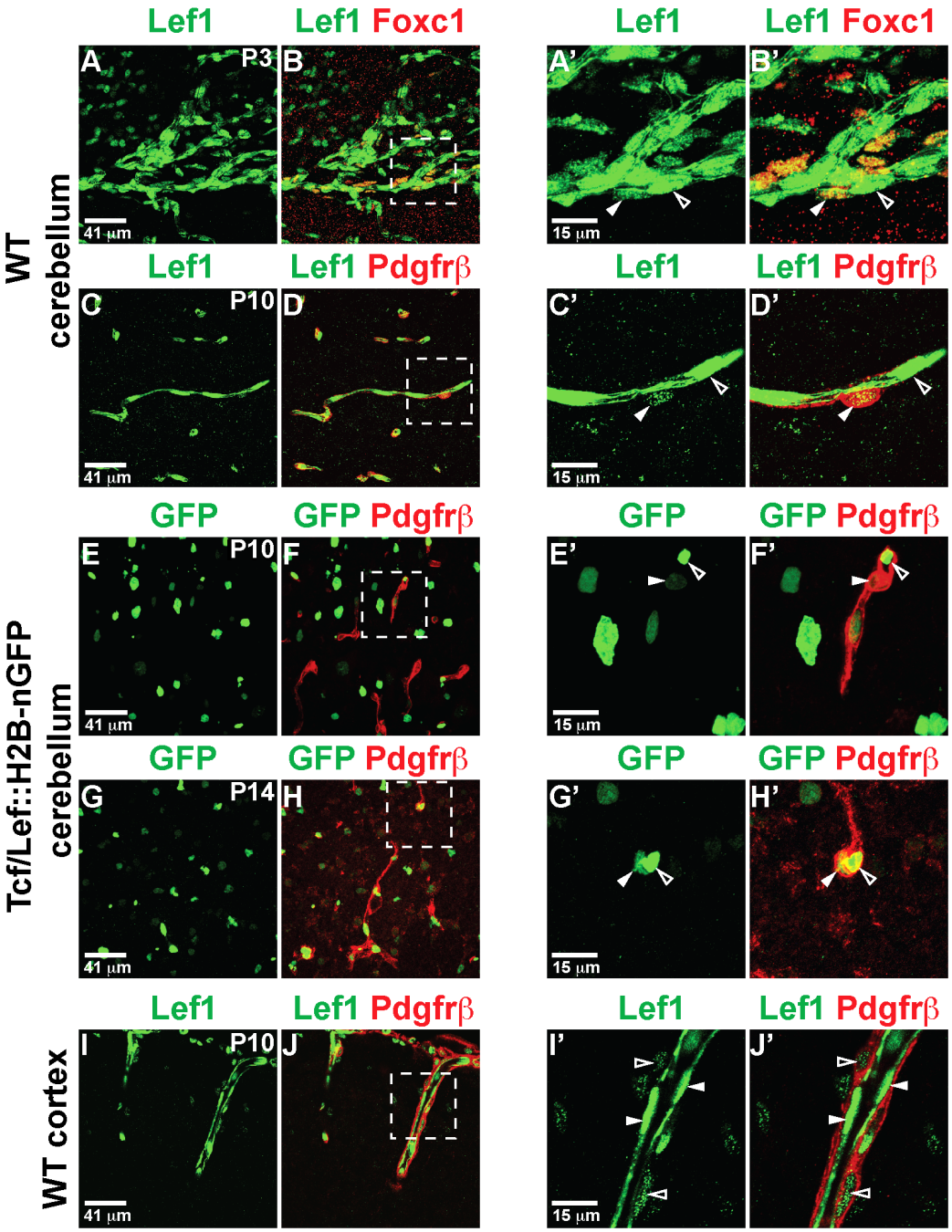

Fig. S2 (related to Figs. 1, 2). Wnt/β-catenin signaling is activated in cerebellar and cortical mural cells. A-B') P3 WT cerebellar sections were stained for Lef1 and Foxc1. **C-D')** P10 WT cerebellar sections were stained for Lef1 and Pdgfrb. **E-H')** P10 and P14 Tcf/Lef::H2B-nGFP cerebellar sections were stained for GFP and Pdgfrb. In all images empty arrowheads point to Lef1$^+$ or GFP$^+$ ECs, whereas solid arrowheads point to Lef1$^+$ or GFP$^+$ mural cells. Scale bars: A-J = 41 μm; A'-J' = 15 μm.

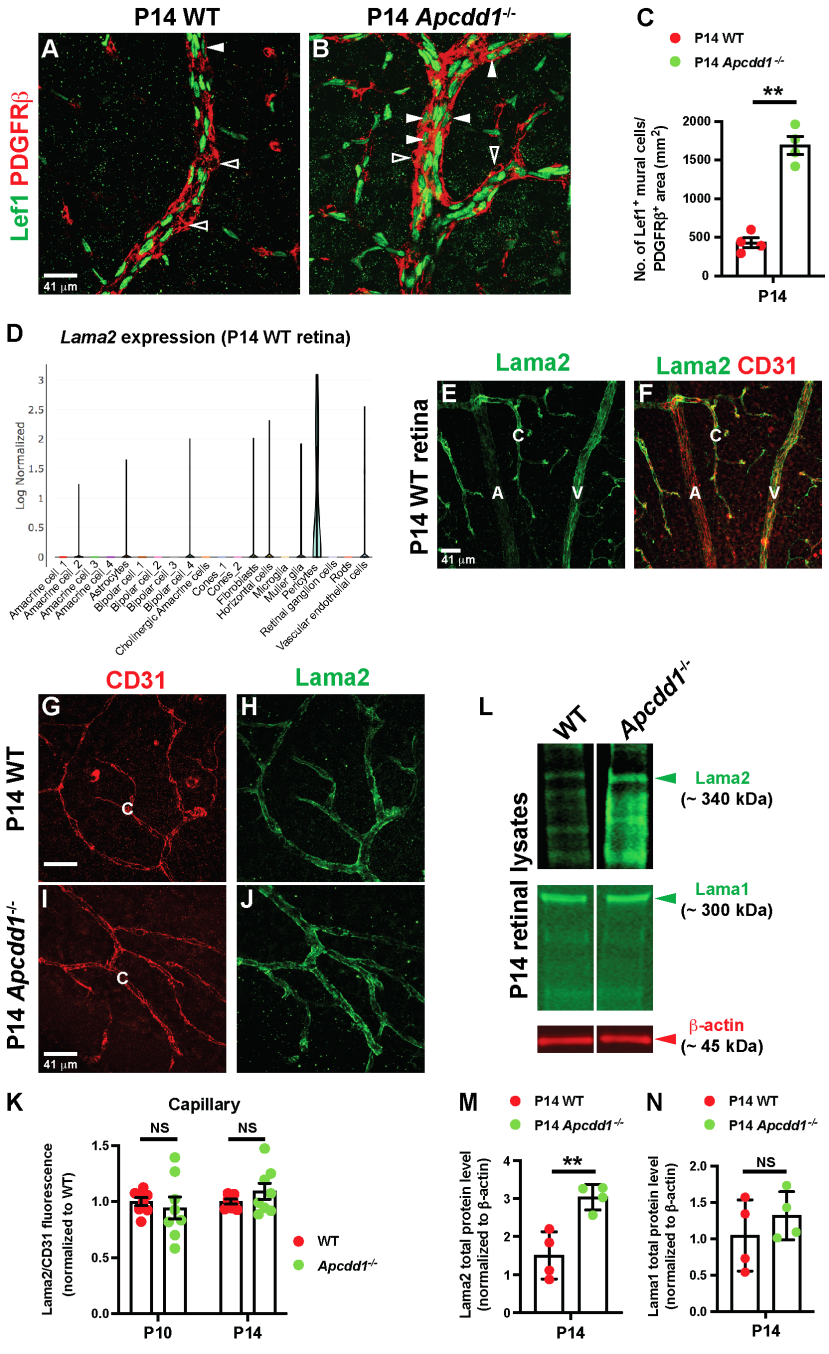

Fig. S3 (related to Fig. 3). Lama2 (*Lama2*) is predominantly expressed in retinal PCs, but not in ECs, and is upregulated in the *Apcdd1*$^{-/-}$ retina. A-C) P14 WT and *Apcdd1*$^{-/-}$ retinal flat-mounts were stained

for Lef1 and Pdgfrβ. Solid arrowheads point to Lef1^{+} mural cells, empty arrowheads point to Lef1^{-} mural cells. Dotted bar graph shows the number of Lef1^{+} mural cells (n=4 animals/genotype). **D)** Expression profile of *Lama2* mRNA in P14 WT retinal cells from the published retina single cell RNAseq database. **E, F)** P14 WT retinal flat mounts were stained for CD31 and Lama2 proteins. A= artery, V= vein, C= capillary. **G-K)** P14 WT and *Apcdd1*$^{-/-}$ retinal flat-mounts were labelled for Lama2 and CD31, showing retinal capillaries (C). Dotted bar graphs show the ratio of Lama2/CD31 M.F.I in capillaries normalized to the WT average values at P10 and P14 (8 fields of capillary network from n=4 mice/genotype). **L)** P14 WT and *Apcdd1*$^{-/-}$ whole retinal lysates were probed for Lama1 or Lama2 (green bands) and β-actin (red bands) by western blot. **M, N)** Quantification of Lama1 and Lama2 protein levels (normalized to β-actin) by western blotting (n=4 samples/group). Student's t-test: **p<0.02, NS= not significant. Graphs show mean+/- SEM (C, K) or mean +/- SD (M, N). Scale bars: 41 μm.

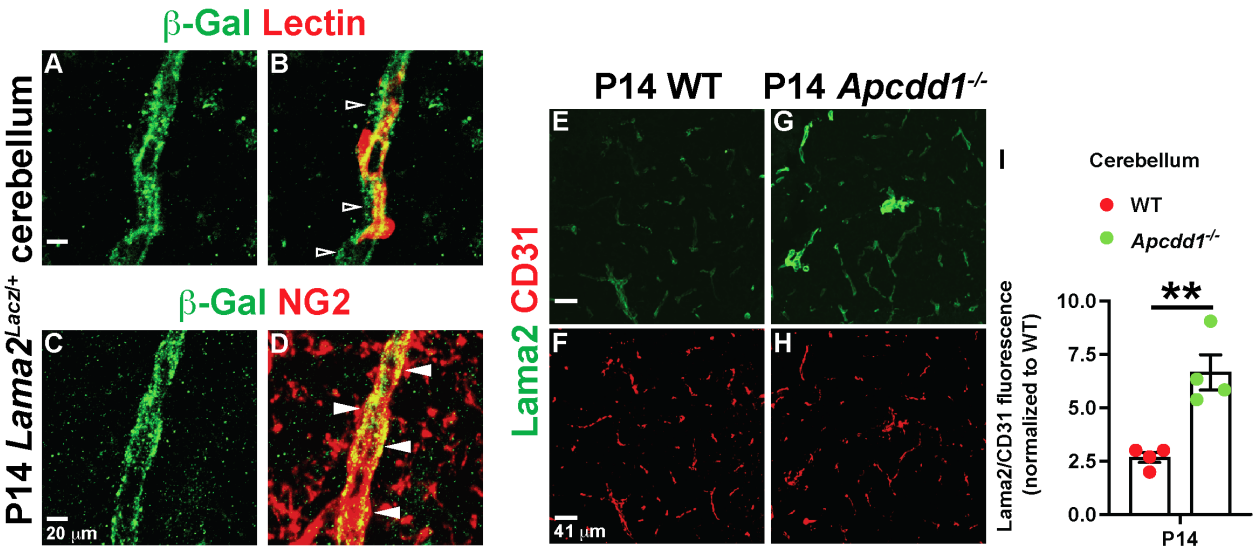

Fig. S4 (related to Fig. 3). Mural cell-derived Lama2 expression and deposition are upregulated in the *Apcdd1*$^{-/-}$ cerebellar vascular basement membrane. **A-D)** P14 *Lama2*$^{Lacz/+}$ cerebellar sections were stained for β-galactosidase (β-Gal) and either Lectin (A-B) or NG2 (C-D). Empty arrowheads point to β-Gal^{-} ECs. Solid arrowheads point to β-Gal^{+} mural cells. **E-I)** P14 WT and *Apcdd1*$^{-/-}$ cerebellar sections were immunolabelled for Lama2 and CD31. Dotted bar graph shows the ratio of Lama2/CD31 M.F.I in, normalized to the WT values (n=4 mice/genotype); Students' t-test: **p<0.02. Graph shows mean+/-SEM. Scale bars: A-D= 20 μm; E-H= 41 μm.

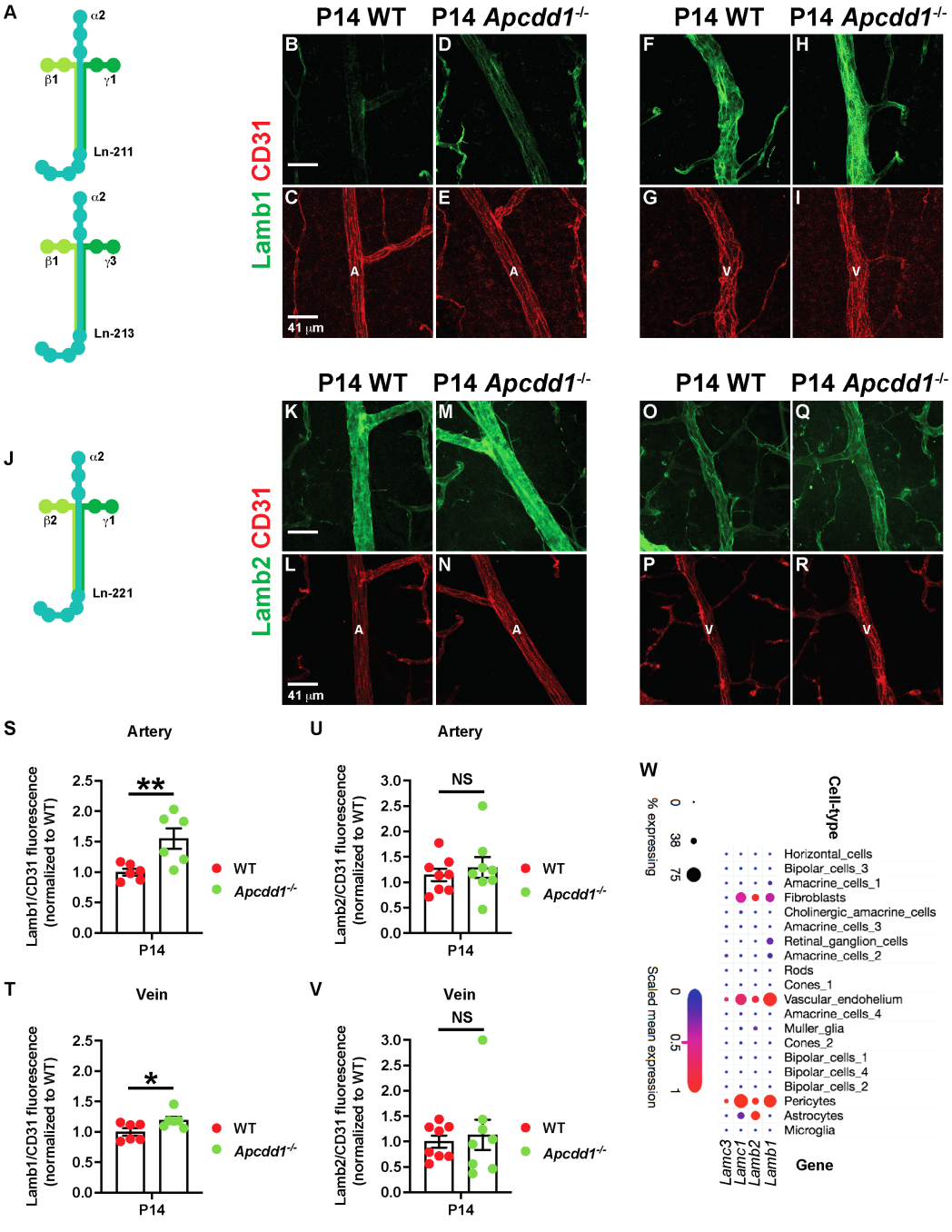

Fig. S5 (related to Fig. 3). Laminin-211 is likely the most affected isoform in the *Apcdd1*$^{-/-}$ retina. A) Schematic diagram of two Laminin heterotrimers (211 and 213) containing α2 and β1. **B-I)** P14 WT and *Apcdd1*$^{-/-}$ retinal flat-mounts were labelled for Lamb1 and CD31. **J)** Schematic diagram of one α2- and β2-

containing Laminin heterotrimer (221). **K-R)** P14 WT and *Apcdd1*$^{-/-}$ retinal flat-mounts were labelled for Lamb2 and CD31. **S, T)** Dotted bar graphs show the ratio of Lamb1/CD31 M.F.I in arteries and veins at P14 normalized to the WT average values (6 arteries or veins analyzed from n=3 mice/group). **U, V)** Dotted bar graphs show the ratio of Lamb2/CD31 M.F.I in arteries and veins at P14 normalized to the WT average values (8 arteries and veins analyzed from n=4 mice/group). **W)** Analyses of the published P14 WT retinal single cell RNAseq database (see Results and Materials and Methods sections) to explore the expression profiles of *Lamb1*, *Lamb1*, *Lamc1*and *Lamc3*. A= artery, V= vein. Student's t-test: *p<0.05, **p<0.02, NS= not significant. Graphs show mean +/- SEM. Scale bars: 41 μm.

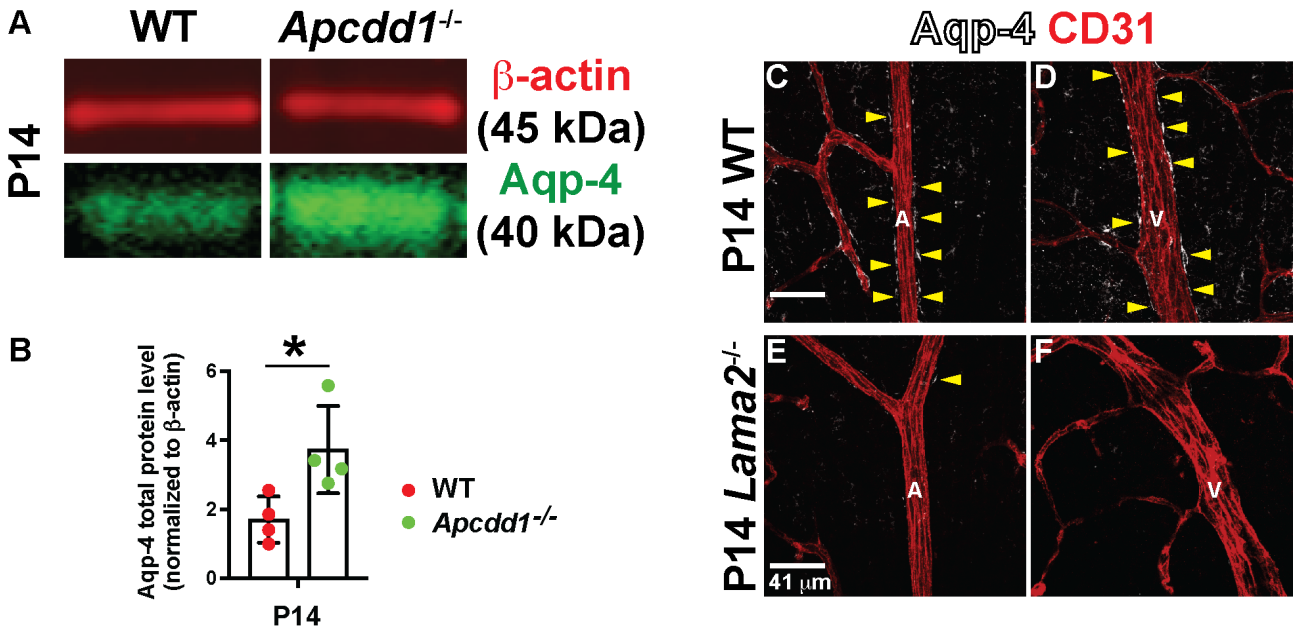

Fig. S6 (related to Fig. 6). Increased Aqp-4 in the *Apcdd1*$^{-/-}$ retina and decreased Aqp-4^{+} astrocyte endfeet polarization in the *Lama2*$^{-/-}$ retina. A) P14 WT and *Apcdd1*$^{-/-}$ whole retinal lysates were probed for Aqp-4 (green bands) and β-actin (red bands) by western blot. **B)** Quantification of Lama1 and Lama2 protein levels (normalized to β-actin) by western blotting (n=4 samples/group). Student's t-test: *p<0.05. Graphs show mean +/- SD. **C-F)** P14 WT and *Lama2*$^{-/-}$ retinal flat-mounts were labelled for Aqp-4 and CD31. Yellow arrowheads point at Aqp-4^{+} astrocyte endfeet around retinal blood vessels. A= arteries and V= veins. Scale bars: 41 μm.

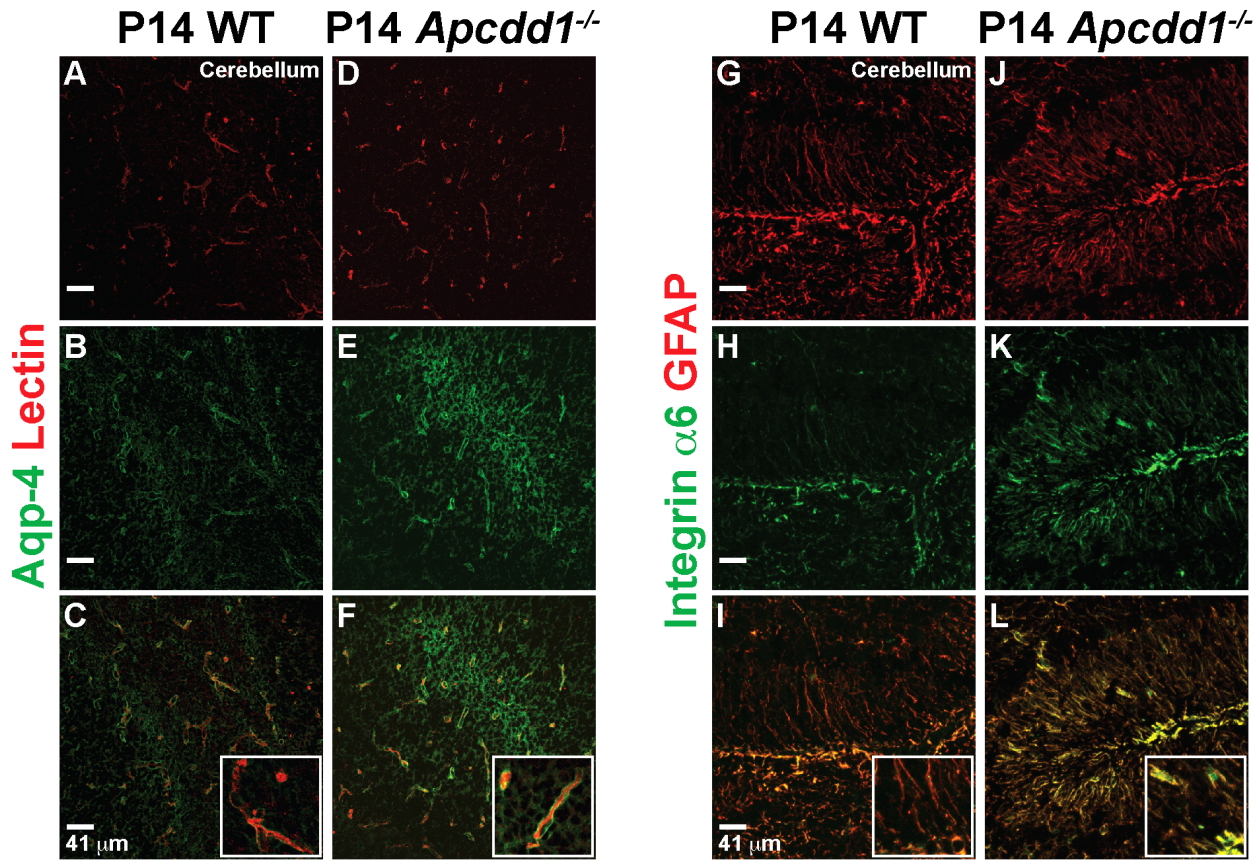

Fig. S7 (related to Figs. 6 and 8). Increased expression of Aqp4 in astrocyte endfeet and Integrin α6 in *Apcdd1*$^{-/-}$ astrocytes in the cerebellum. A-F) P14 WT and *Apcdd1*$^{-/-}$ cerebellar sections were labelled for Aqp-4 and Lectin. Insets show higher magnification images of single vessels. **G-L)** P14 WT and *Apcdd1*$^{-/-}$ cerebellar sections were labelled for Integrin α6 and GFAP. Insets show higher magnification images. Scale bar: 41 μm.

Table S1 (related to Figs. 2, 3, 6 and 8). List of significantly differentially expressed genes between wild-type and *Apcdd1*$^{-/-}$ retinas at P10 and P14. Negative values mean that the gene is lower in *Apcdd1*$^{-/-}$ compared to wild-type retinas, and positive values mean that the gene is higher in *Apcdd1*$^{-/-}$ compared to wild-type retinas.

Click here to download Table S1

Table S2 (related to Fig. 2). List of significant differentially expressed putative endothelial genes between wild-type and *Apcdd1*$^{-/-}$ retinas at P10 and P14. The genes are ranked by $\log_2$Fold Change from the lowest to the highest value. Negative values mean that the gene is lower in *Apcdd1*$^{-/-}$ compared to wild-type retinas, and positive values mean that the gene is higher in *Apcdd1*$^{-/-}$ compared to wild-type retinas.

Click here to download Table S2

Table S3 (related to Figs. 2 and 3). List of significant differentially expressed putative pericyte genes between wild-type and *Apcdd1*$^{-/-}$ retinas at P10 and P14. The genes are listed by $\log_2$Fold Change from the lowest to the highest value. Negative values mean that the gene is lower in *Apcdd1*$^{-/-}$ compared to wild-type retinas, and positive values mean that the gene is higher in *Apcdd1*$^{-/-}$ compared to wild-type retinas.

Click here to download Table S3

Table S4 (related to Figs. 2, 3 and 8). List of significant differentially expressed extracellular matrix genes (ECM) between wild-type and *Apcdd1*$^{-/-}$ retinas at P10 and P14. The genes are listed by log_2Fold Change from the lowest to the highest value. Negative values mean that the gene is lower in *Apcdd1*$^{-/-}$ compared to wild-type retinas, and positive values mean that the gene is higher in *Apcdd1*$^{-/-}$ compared to wild-type retinas.

Click here to download Table S4

Table S5 (related to Fig. 6). List of significant differentially expressed astrocyte maturity genes between wild-type and *Apcdd1*$^{-/-}$ retinas at P10 and P14. The genes are listed by log_2Fold Change from the lowest to the highest value. Negative values mean that the gene is lower in *Apcdd1*$^{-/-}$ compared to wild-type retinas, and positive values mean that the gene is higher in *Apcdd1*$^{-/-}$ compared to wild-type retinas.

Click here to download Table S5